Soil Dynamics and Earthquake Engineering 203 (2026) 110079

Contents lists available at ScienceDirect

Soil Dynamics and Earthquake Engineering

journal homepage: www.elsevier.com/locate/soildyn

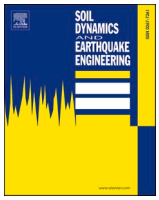

Novel seismic Dam Damage Intensity scale and empirical models for predicting seismically induced damages in embankment dams

P. Anbazhagan *, Surya Prakash

Department of Civil Engineering, Indian Institute of Science, Bangalore, Karnataka, India

ARTICLE INFO

Keywords:
Earthquake damage
Dam damage intensity (DDI) scale
Damage assessment
Embankment dams
Modified mercalli intensity
Seismic vulnerability

ABSTRACT

Earthquakes pose significant risks to dam safety and jeopardize lives. Current damage assessment methods lack a standardized scale for classifying seismic damage to embankment dams, and the Modified Mercalli Intensity (MMI) scale falls short in addressing the complexities of dam damage. This study introduces: (1) a novel Dam Damage Intensity (DDI) scale, specifically designed to quantify earthquake-induced damage to embankment dams, and (2) novel empirical DDI predictive models that integrate seismic parameters: magnitude (M_w) and hypocentral distance (R_{hyp}) with dam characteristics: height (H_D), age (A_D), and dam type (DT). The DDI scale classifies damage into five levels, from minor (1) to complete failure (5). Based on the analysed dataset of 109 dams affected by 16 earthquakes, potential seismic damage is associated with $M_w \geq 6.0$ and $R_{hyp} \leq 250$ km. Four functional forms of DDI predictive models were evaluated: two based on modified Intensity Prediction Equations (IPE) (Models 3 & 4), one from modified Ground Motion Prediction Equations (Model 2), and one from a modified dam crest settlement model (Model 1). IPE models consistently outperformed the others, achieving the highest R^2 (≈0.62), lowest errors (MSE = 0.79, RMSE = 0.89, MAE = 0.75), and minimal log-likelihood value (1.300–1.302), and exhibited consistent predictive performance under repeated out-of-sample validation. Sensitivity analysis revealed that R_{hyp} and H_D are the most influential seismic and dam parameters respectively, contributing to DDI predictions. DDI scale and predictive models offer a reliable tool for preliminary damage assessment for embankment dams in earthquake-prone regions.

1. Introduction

Embankment dams represent the predominant form of dam constructed globally, comprising approximately 70 % of all existing dams [1,2]. These vital infrastructures fulfill a diverse array of functions, including flood mitigation, irrigation, water resource management, and hydroelectric power generation [3]. Typically constructed from natural materials such as soil, rock, and clay, the common types of embankment dams include earthfill, homogeneous earth, and rockfill dams [4]. However, the integrity of these structures can be severely challenged by seismic events, which may lead to catastrophic failures and pose significant risks to human safety and property [5]. Understanding the impact of seismic activity on embankment dams is, therefore, crucial for safeguarding these essential infrastructures.

Historical incidents highlight the vulnerability of embankment dams to earthquakes [6–10]. The Lower San Fernando Dam in California nearly collapsed during the 1971 earthquake, leading to improved design practices for earthquake resistance [11]. The 2011 Tōhoku earthquake in Japan raised concerns about the stability of these dams, calling for thorough assessments of their seismic resilience [12]. Most recently, the M_w 7.8 earthquake in Turkey on February 6, 2023, impacted over 100 dams, showing varying damage levels [13]. These events have spurred ongoing research into the seismic vulnerabilities of embankment dams to enhance future design and safety measures.

Assessing damage from seismic events in embankment dams presents several challenges that current damage assessment methods struggle to address. Established scales, such as the Modified Mercalli Intensity (MMI) scale, provide a qualitative assessment of earthquake intensity on a scale from I (not felt) to XII (complete destruction), heavily relying on personal observations from those who experienced the tremor [14]. Similarly, the European Macroseismic Scale (EMS) offers criteria for evaluating earthquake effects on buildings [15]. The damage ratio method further contributes to the analysis by comparing repair costs to the pre-earthquake value of the building, serving an important role in insurance and economic evaluations [16].

Despite enhancements made to the MMI scale by studies such as

* Corresponding author.
E-mail address: anbazhagan@iisc.ac.in (P. Anbazhagan).

https://doi.org/10.1016/j.soildyn.2025.110079
Received 24 October 2025; Received in revised form 18 December 2025; Accepted 30 December 2025
Available online 5 January 2026

Dowrick [17], it remains inadequate for evaluating damages to critical infrastructure, including embankment dams, due to its subjective nature and limitations at high-intensity levels. Anbazhagan et al. [18] highlighted these shortcomings in assessing road damage from earthquakes and proposed a new damage scale to quantify such impacts. A significant limitation of the MMI when assessing damage to embankment dams is its failure to account for critical factors such as dam type and design, which are essential for an accurate evaluation of seismic responses. Additionally, the MMI's reliance on surface observations often overlooks internal damage or structural failures that may occur within these structures. As the need for comprehensive assessment methods intensifies in the wake of increasing seismic activity, addressing these gaps is crucial for enhancing the resilience and safety of embankment dams.

Furthermore, studies have proposed damage classification methodologies and scales for structures such as reinforced concrete, bridges, and masonry buildings [19–21]. These methodologies enable effective evaluation of performance during earthquakes [22–25]. Current guidelines and frameworks provide practitioners with the necessary tools to assess the seismic damage classifications and damage scaling of these structures [22,26]. However, there is a significant gap in the study on comparable damage classification systems and damage scales for embankment dams, which are also vulnerable to seismic risks. The lack of dedicated damage classification methodologies and damage scales for embankment dams highlights the need for further research to create an effective damage scale that addresses their unique vulnerabilities and performance characteristics during seismic events [22,27,28]. Developing such a scale would enhance our understanding of the seismic risks of embankment dams, ultimately contributing to improved safety and resilience in earthquake-prone regions.

This paper introduces a novel seismic damage scale called the seismic Dam Damage Intensity (DDI) scale. DDI is developed to address the limitations of existing seismic damage assessment scales, such as the MMI. DDI is designed specifically to quantify earthquake-related damage to dams using historical earthquake records, offering a more effective framework for qualitatively evaluating their structural integrity under seismic activity. MMI and the DDI are plotted against earthquake parameters, i.e., magnitude and hypocentral distance, to determine which damage intensity scale correlates best with these parameters. Additionally, we propose empirical DDI predictive models designed to predict damage induced due to earthquakes in embankment dams. These models integrate earthquake-related parameters, i.e., Magnitude (M) and Hypocentral Distance (R_{hyp}), alongside dam-specific characteristics such as Height (H_D), Age (A_D), and Dam Type (DT), and give the DDI predictions. We evaluate four functional forms for the predictive models: two based on modified Intensity Prediction Equations (IPE), one derived from modified Ground Motion Prediction Equations (GMPE), and another based on a modified dam crest settlement model. An analysis of the contributions of each predictor variable to DDI predictions is performed to identify key factors influencing DDI outcomes. By introducing the DDI scale and DDI predictive models, this study aims to improve the accuracy of seismic damage assessments and advance the overall understanding of seismic risk management for embankment dams. The novel contributions of this work are: 1) Development of the Dam Damage Intensity (DDI) scale to classify the seismic damages in embankment dams; 2) Development of empirical DDI predictive models using seismic and dam parameters; 3) Evaluation of the contribution of predictor variables in the DDI predictions.

2. Seismically damaged dam dataset

We compiled a dataset of embankment dams that sustained damage during past earthquakes from a wide range of literature sources and historical records. Although numerous earthquakes have been reported to cause structural damage to dams, detailed documentation, particularly in the form of photographs and comprehensive descriptions, remains limited. This lack of systematic reporting poses challenges for researchers and engineers seeking to assess dam performance under seismic loading.

The dataset incorporates both earthquake-related and dam-specific parameters. Earthquake characteristics include moment magnitude (M_w), epicentral distance (R_{epi}), and focal depth (D_f). Wherever available, MMI values at the dam sites were also collected. Dam parameters include height of dam (H_D) and age of dam (A_D). Damage descriptions were verified against photographic evidence when possible to ensure consistency and reliability. In total, the dataset covers 16 earthquake events, yielding 109 documented cases of damage to earthen dams. Table 1 summarises the earthquake events considered in this study and forms the basis for the development of the proposed damage intensity scale and predictive model. A detailed account of individual earthquakes and associated dam damage is provided in the supplementary dataset (Table S_1). Fig. 1 shows the global distribution of earthquake events included in the compiled dataset. These damaging events occur across several major seismically active regions, China, Japan, Turkey, the United States, India, and the Philippines, demonstrating that the dataset is not confined to a single geographic or tectonic context. For each region, the number of affected dams and corresponding earthquake magnitudes are summarised, illustrating the range of seismic loading conditions represented. The documented events span magnitudes of M_w 6.7–8.0, hypocentral distances (R_{hyp}) of 15–234 km, and focal depths of 6–62.9 km. Although earthquake-induced dam-damage cases remain globally sparse, the dataset incorporates observations from multiple continents, diverse tectonic regimes, and different dam portfolios. Because MMI values were not available for every site, they are reported for 78 dam locations only, as indicated in Table S_1 (Supplementary dataset).

3. Seismic Dam Damage Intensity Scale

Historical documentation of earthquake-induced dam damage is predominantly qualitative, relying on narrative descriptions, photographic evidence, and non-standardised engineering notes. The dataset compiled for this study includes 109 such cases, encompassing cracking, leakage, deformation, settlement, slope movement, and operational disturbances. This heterogeneity, combined with the fundamentally different seismic response of dams compared with buildings or lifelines, necessitates a dedicated, standardised approach for translating descriptive observations into a consistent classification system. Existing macroseismic intensity scales, such as the Modified Mercalli Intensity (MMI), are insufficient for this purpose: they describe general shaking effects at the community scale and provide only coarse references to dams at very high intensity levels (e.g. “damage serious to dams, dikes, embankments” at MMI X and “great damage to dams” at MMI XI) [14]. Such general intensity scales are not tailored to structures like dams, tunnels, and roads and lack the structural resolution needed for engineering analyses [18,35,36].

The Dam Damage Intensity (DDI) scale is introduced to address these limitations. DDI is a structured, dam-specific framework designed to enable reproducible classification of seismic damage. The need for DDI arises directly from the qualitative nature of historical damage records and the lack of dam-focused criteria in general intensity scales. The DDI scale establishes explicit, rule-based physical criteria for assigning damage levels, thereby minimising subjective interpretation. These criteria include quantitative ranges for crack width and depth, classifications of leakage severity, thresholds for measured deformation or displacement (e.g., crest settlement or lateral movement), observable indicators of slope instability, and post-earthquake operability or repair requirements. Each indicator is defined through clear numerical or categorical thresholds derived from documented dam case histories [31,37] and international best-practice guidance for empirical damage assessment [38]. Because the criteria are explicitly specified, consistent application of the rules ensures that independent evaluators would assign the same DDI level for the same set of observations, thereby

Table 1
List of earthquake events used for the scale development.

Earthquake Name	Date	Epicentre		M_w	Depth (km)	Number of Dams	References
		Lat(°N)	Long(°E)				
Nigata Earthquake	June 16, 1964	37.8	139	7.6	10	1	[29]
Santa Barbara Earthquake	June 29, 1925	34.3	−119.8	6.8	10	1	[29]
Imperial Valley Earthquake	June 22, 1915	32.75	−115.3	6.9	6	1	[30]
Hebgen Lake Earthquake	August 18, 1959	44.863	−111.335	7.2	25	1	[30]
Tokai-oki Earthquake	May 16, 1968	40.9	143.35	7.9	26	1	[29]
Hokkaidou Nanseioki Earthquake	July 2, 1973	43.233	145.785	7.8	48	1	[29]
Miyagi-Oki Earthquake	June 12, 1978	38.15	142.2167	7.4	30	2	[29]
Nihonkai-Chubu Earthquake	May 26, 1983	40.4	138.91	7.9	24	3	[29]
Chiba-Touhouoki Earthquake	December 17, 1987	35.372	140.519	6.7	62.9	1	[29]
Philippines Earthquake	July 16, 1990	15.7	121.1167	7.7	25.1	1	[29]
Northridge Earthquake	January 17, 1994	34.213	−118.537	6.7	18.2	1	[31]
Kobe Earthquake	January 16, 1995	34.6	135	6.9	22	1	[29]
Bhuj Earthquake	January 26, 2001	23.4	70.28	7.7	25	4	[32]
Wenchuan Great Earthquake	May 12, 2008	30.989	103.329	8	19	66	[33]
Pazarcık Earthquake	February 6, 2023	37.288	37.043	7.7	8.6	9	[34]
Elbistan Earthquake	February 6, 2023	38.089	37.239	7.6	7	11	[34]

Abbreviations: Lat: Latitude, Long: Longitude, M_w: Moment Magnitude.

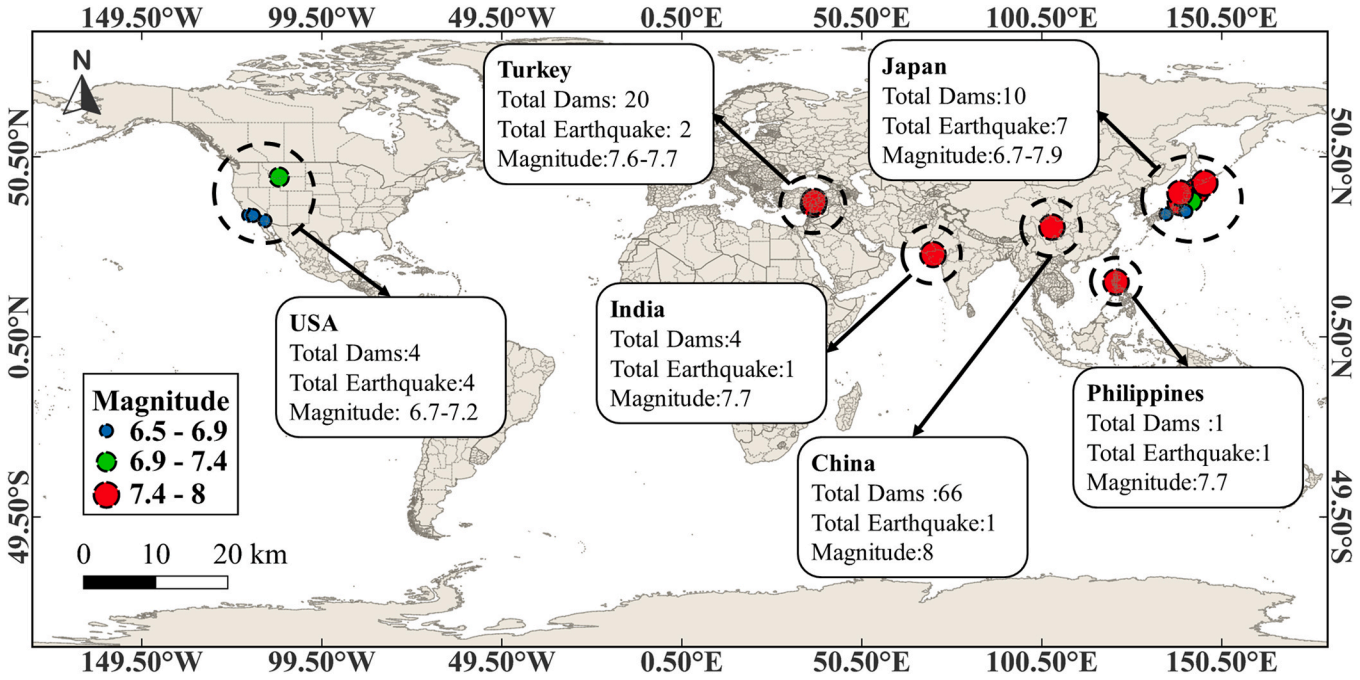

Fig. 1. Map illustrating the location of the epicentre of earthquakes considered in DDI scale development.

improving reproducibility and reducing ambiguity in empirical damage classification.

DDI levels are assigned directly from observed damage descriptors and are not derived from MMI or any other seismic parameter. Consequently, historical damage records were not reclassified from MMI to DDI, and MMI values are reported solely for contextual comparison. This direct assignment from observed damage ensures that subsequent analyses, such as correlation or regression using DDI, remain free from circular reasoning. The DDI scale defines five levels of damage severity (I–V), capturing the full spectrum of seismic effects relevant to embankment dams. Primary seismic effects include deformation, settlement, tilting, longitudinal cracking, leakage, and sliding, while secondary effects, such as liquefaction and earthquake-induced landslides, are also incorporated. These mechanisms represent well-documented precursors to functional impairment and, at higher levels, structural failure. Table 2 summarises the detailed criteria associated with each DDI level, ranging from minor, non-structural impacts at Level I to complete structural destruction at Level V. Representative photographic evidence illustrating these levels is provided in Fig. 2. By relying on measurable indicators and focusing on observable structural behaviour, the DDI scale establishes a transparent, reproducible, and engineering-relevant framework for evaluating seismic damage to embankment dams. This contributes to a more rigorous understanding of dam vulnerability and performance under earthquake loading.

4. Classification of damaged dams

In this section, we compile observed cases of seismic dam damage documented in historical records. Concurrently, earthquake parameters and dam characteristics, including DT, H_D, and A_D, were extracted from these sources. Reported MMI intensity at the dam site was also extracted from these sources for contextual comparison with DDI. A comprehensive analysis of all recorded instances of dam damage was conducted, leading to the systematic reclassification of the dams according to the

Table 2
Proposed Dam Intensity Scale to define seismic damage of Embankment Dams.

DDI Level	Damage Description	Post-Earthquake Functional Condition	Typical Historical Context[a]	Reported MMI in Historical Records[a]
1	Slight Damage: Damage is limited to minor superficial cracks (width <1 cm, depth <1 m) with no leakage, subsidence, or structural damage to auxiliary facilities.	Fully operational; only minor cosmetic repairs needed.	Often observed in relatively modern dams located at larger epicentral distances, where shaking levels were light to moderate.	XI, VII, VIII, VI
2	Minor Damage: Minor cracks along the crest (width <5 cm, depth 1–2 m), slight leakage, and no signs of subsidence or slope failure are observed.	Operational; minor repairs required to restore initial condition.	Reported in dams constructed in the mid-20th century, located at moderate distances from the epicentre and subjected to moderate shaking.	VI, VII, VIII
3	Medium Damage: Small to medium cracks (5–10 cm wide, 2–3 m deep), slight to medium leakage, and signs of subsidence without major slope failure. Possible damage to auxiliary facilities.	Operation restricted; substantial repairs required before resuming normal use.	Typically observed in embankment dams constructed before the adoption of modern seismic design practices, located at moderate to relatively short distances from the epicentre, where shaking was strong.	VIII, IX, X, VI
4	Serious Damage: Large cracks (width >10 cm, depth >3 m), significant leakage, signs of landslides or tilting, and localized displacement. Dams are severely damaged but not failed and require immediate partial seismic retrofitting.	Dam crest generally closed to vehicle access; major structural repairs required.	Frequently associated with dams constructed without formal seismic design provisions, located near the epicentre and exposed to very strong shaking.	X, XI, VII, VI, VIII
5	Severe damage or failure: Signs include major displacements, tilting, significant cracks (depth >5m, width >15 cm), and severe leakage. Complete collapse and liquefaction.	Full closure required; emergency response and major reconstruction.	Observed in dams lacking seismic design considerations, typically located close to the epicentre, where shaking intensity was extreme.	X, VII, VIII, VI

[a] Historical context and historical MMI values are provided only for descriptive purposes and were not used in assigning DDI levels.

newly proposed DDI scale, as summarised in the supplementary dataset (Table S_1). In the classification process, damaged embankment dams have been categorized into three principal types: homogeneous earth dams (HED), rockfill dams (RFD), and earth-fill or earth-cored dams (CED), based on their materials and construction method. The dataset was carefully refined to ensure that each dam type incorporates critical earthquake parameters (M_w, R_{epi}, and D_f) along with relevant dam characteristics (H_D, A_D) necessary for developing a functional DDI predictive model. In Fig. 3, the dataset for embankment dams is summarised, along with the new DDI scale classifications. The finalized dataset, which will serve as the foundation for developing predictive models for DDI, is presented in the supplementary dataset (Table S_1).

Fig. 4 presents histograms illustrating the frequency distributions of key variables in the dataset, summarising the main predictors and response used in the analysis. Earthquake parameters (M_w and R_{hyp}) span a wide range of shaking intensities, with M_w mostly between 6.5 and 8 and R_{hyp} from 15 m up to 234 km. In the dam-related variables, heights range from 5 m to 105 m, with most cases below 40 m, and ages vary from newly constructed to over 120 years. Categorical variables include three dam types (HED, CED, RFD), while DDI values cover all defined damage levels (DDI1–DDI5), with lower levels being more frequent. It is important to note that MMI values are not uniformly documented for all individual dams or their specific geographic locations. In many cases, multiple MMI values correspond to a single DDI value, as shown in Table 2, which aligns with the definitions of the new DDI scale. Fig. 5a–d illustrate the relationships of MMI and DDI with key earthquake parameters across all embankment dam types, offering qualitative insight into their observed behaviour. Specifically, Fig. 5a shows that MMI data are incomplete for certain magnitudes, and no discernible trend with earthquake magnitude (M_w) is apparent. In contrast, Fig. 5b demonstrates that DDI values are available across all magnitudes, revealing a significant and consistent trend when appropriately grouped. Similarly, Fig. 5c highlights the limited availability of MMI data across a broad range of R_{hyp}, with no clear trend observed. By comparison, Fig. 5d shows that DDI values cover a wide range of R_{hyp}, exhibiting a distinct and consistent trend. These observations are consistent with the findings of [18], which reported no clear trend of MMI with either M_w or R_{hyp} when classifying seismic road damage, further supporting the limited applicability of MMI for dam-specific seismic assessments.

The consistent trends observed for DDI with seismic parameters in Fig. 5b and Fig. 5d reflect the scale's intrinsic design. Because DDI is defined exclusively from observable structural damage descriptors such as crack width and depth, seepage severity, slope deformation, crest settlement, and operational impairment, it represents a dam-specific engineering damage state rather than a shaking-intensity metric. DDI is therefore expected to exhibit stronger statistical links to seismic loading than a generic intensity measure (e.g. MMI) not tailored to dams. By contrast, MMI is a community-based shaking intensity scale describing general effects on people and buildings, with only limited reference to dam damage at very high intensities (MMI X) [14]. A stronger statistical association between DDI and seismic parameters is therefore expected and does not arise from circularity or reclassification bias. Nevertheless, all observed trends are constrained by the sparse and heterogeneous nature of historical damage documentation, which introduces inherent epistemic uncertainty [38].

Analysis of the dataset indicates that the minimum earthquake magnitude associated with observed dam damage is M_w 6.5, while the maximum hypocentral distance is 250 km. This observed lower bound of M_w 6.5 should not be interpreted as a universal threshold, but rather reflects the characteristics and completeness of the compiled historical dataset. Based on these observations, we also recommend an M_w of 6.0 and a maximum R_{hyp} of 250 km from the dam site to the epicentre during an earthquake event in which seismic damage to the dam may occur. It should be noted that dam damage may also result from secondary effects such as tsunamis, seiches, or cascading failures of

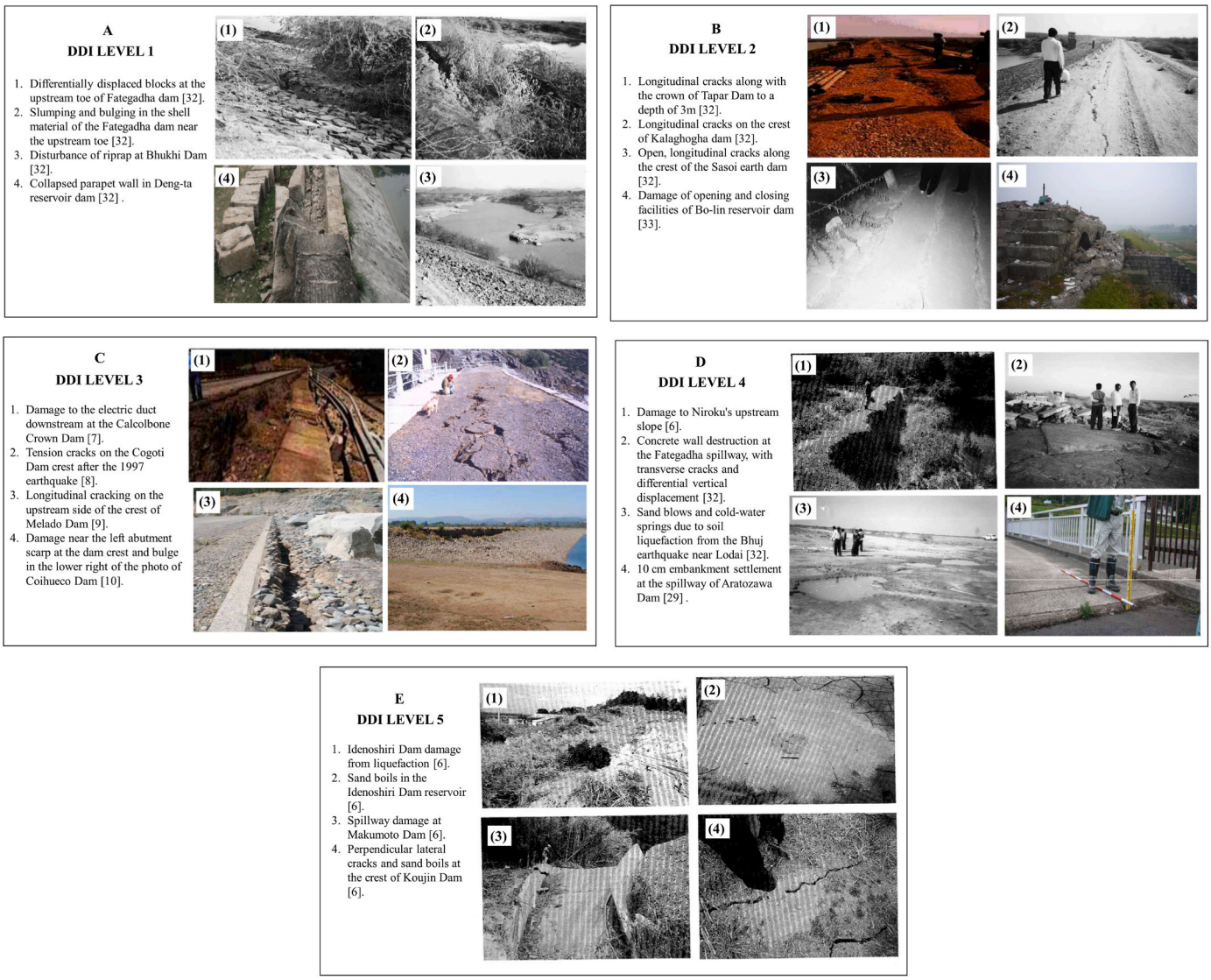

Fig. 2. Representative photographs illustrating common failures for each DDI Level.

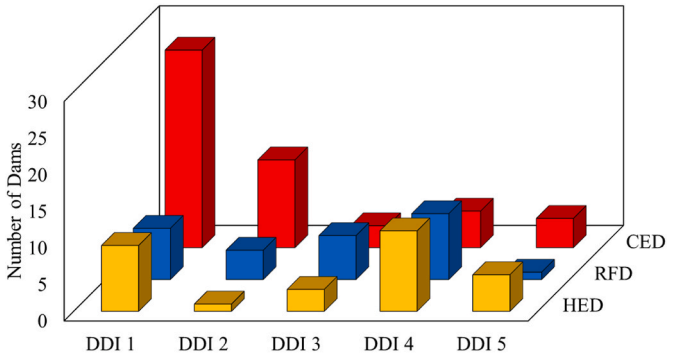

Fig. 3. Number of dams corresponding to each DDI and the dam types (homogeneous earth dams (HED), rockfill dams (RFD), and earth-fill or earth-cored dams (CED)).

upstream dams. Although specific reports of such events were not included in our dataset, comprehensive risk assessments should account for these factors. Consequently, dams located near the sea, downstream of other dams, or adjacent to unstable upstream slopes may require consideration of larger distances for accurate seismic risk evaluation.

Overall, analysis of Fig. 5a–d demonstrates that the proposed DDI scale exhibits a strong correlation with earthquake parameters, confirming its robustness and suitability for seismic risk assessment of embankment dams and at the same time it should be noted that all comparisons between DDI and MMI are based on historical damage reports and remain subject to substantial epistemic uncertainty due to sparse and heterogeneous data [38]. Global records of earthquake-induced embankment dam damage are limited, often containing only a few dozen well-documented cases, with many events reporting minimal or no damage [31]. Consequently, the dataset is small, geographically uneven, and dominated by narrative descriptions, which may introduce sampling bias and limit generalisability.

5. DDI predictive parameters and model

Seismic damage to earth dams is influenced by multiple factors, including earthquake, site subsurface and dam parameters. Seismic parameters of source, path, and energy released are represented by earthquake size, distance, and source type. Site parameters from the base of the dam to non-amplifying layers can be represented by the average shear wave velocity. Dam parameters include age of dam (A_D), height of dam (H_D), dam type (DT) and stiffness of foundation and dam. Among these parameters, the dam damage reports consist of earthquake

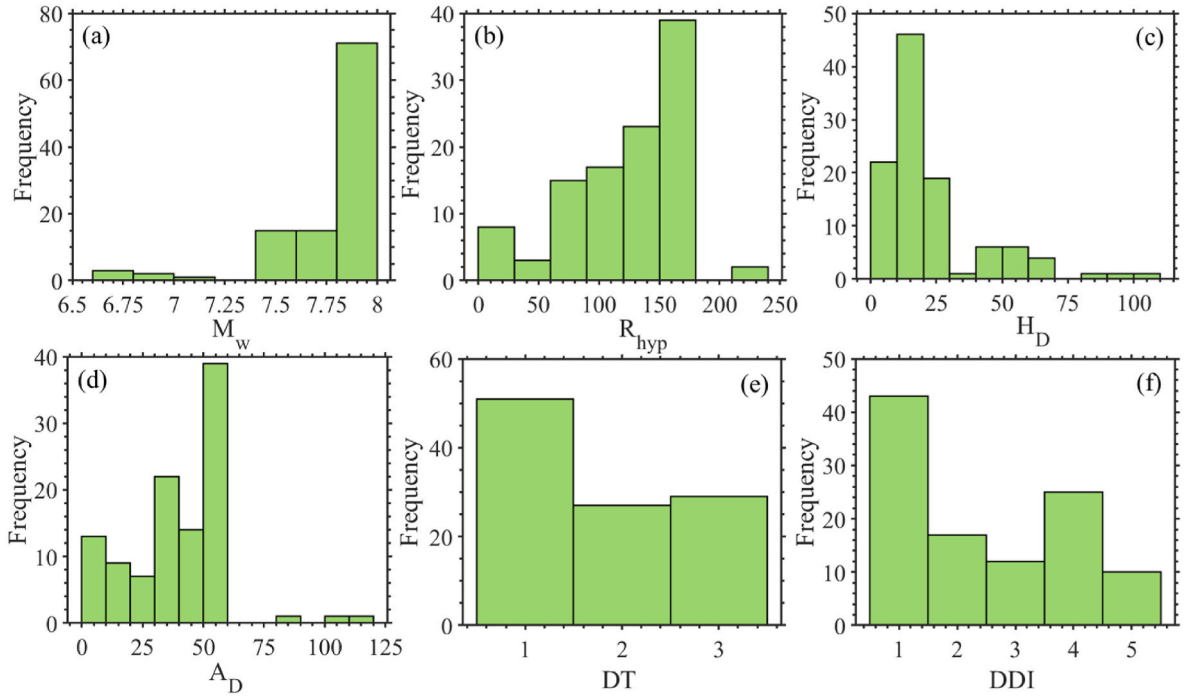

Fig. 4. Histograms showing the frequency distribution of key parameters in the dataset: (a) moment magnitude (M_w); (b) hypocentral distance (R_{hyp}); (c) dam height (H_D); (d) dam age (A_D); (e) dam type (DT); (f) Dam Damage Intensity (DDI).

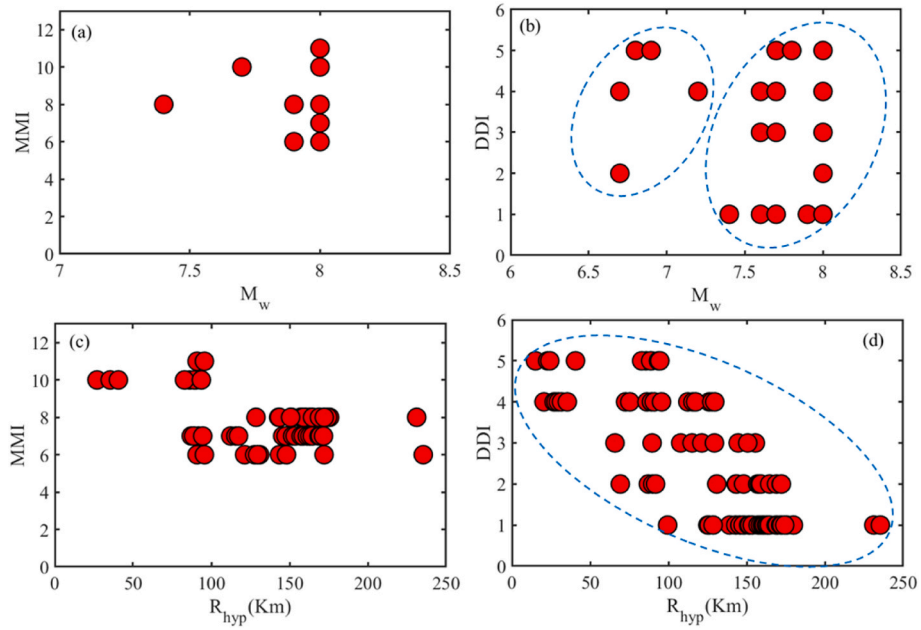

Fig. 5. a) Plot of MMI versus magnitude (M_w); b) Plot of DDI versus magnitude (M_w); c) Plot of MMI versus hypocentral distance (R_{hyp}); d) Plot of DDI versus hypocentral distance (R_{hyp}).

moment magnitude (M_w) and hypocentral distance (R_{hyp}) arrived from the shortest epicentral distance (R_{epi}) and depth of earthquake and dam parameters, including age of dam (A_D), height of dam (H_D) and dam type (DT) are found along with damage description and damage images. Hence, in this study, we considered a total of five predictor variables obtainable from old damage reports to develop the DDI predictive model. The predictive model integrates seismic parameters and dam-specific features to comprehensively assess factors influencing DDI.

The ageing process influences material properties, soil compaction, and overall structural stability [39]. Older dams are generally more susceptible to seismic loading due to factors such as soil degradation, increased pore pressures, and heightened liquefaction potential [40]. In embankment dams, long-term ageing can reduce density, amplifying accelerations and displacements, and promoting plastic deformation within the core [41]. Material deterioration further decreases dynamic resistance, increasing the likelihood of damage [42]. The effects of ageing, however, vary by dam type: homogeneous dams are prone to degradation from seepage, cracking, and cumulative damage, while rockfill dams may experience gradual compaction and enhanced stability through creep or dynamic settlements [43]. Earth-cored dams

exhibit intermediate behaviour, reflecting a combination of consolidation and potential long-term weakening. These differences highlight the importance of incorporating both dam type and age when predicting DDI [44]. However, the data regarding how the material property of dams changes with time is not available in the literature.

Stiffness in terms of seismic velocity of compressional and shear waves can represent these characteristics very well, but very limited studies are available in this context. Furthermore, complied damaged dam dataset considered age as the interval between the year of construction and the year of the seismic event. Stiffness is somewhat represented in dam height, which accounts on seismic energy absorption and structural resilience, with taller dams generally presenting higher sliding and overturning risks [42–44]. Height was measured from the crest to the lowest point of the original streambed, or, if unavailable, from the lowest point of the downstream toe [48]. Although the critical section height may differ from the maximum height, consistent data were lacking; thus, the reported dam height was used. Dam type distinguishes between earthen, rockfill, and earth-cored embankment dams, each characterized by unique material properties, construction techniques, and seismic performance. In this study, to capture the effect of different types of embankment dams, the variable dam type (DT) was incorporated into the regression models.

Detailed geotechnical and seismic variables, such as ground-motion frequency content or foundation stiffness, were not incorporated in the DDI predictive model because these data are rarely available for broad, global dam inventories [31,49]. In their absence, we use proxies H_D, A_D, and DT that correlate empirically with historical failure trends and overall structural vulnerability. For example, A_D reflects the cumulative effects of long-term consolidation, cracking, seepage evolution, and construction-era design practices, which are widely documented in literature [30], but no explicit material decay law is assumed. While these proxies cannot capture all site-specific response mechanics, they provide a practical and physically informed means of screening and prioritising dams for further investigation. Once high-risk dams are flagged, detailed geotechnical and seismic analyses (e.g., finite-element modelling of the dam) can follow for those dams to refine risk estimates [50]. To address potential overfitting, the final dataset includes only cases for which complete information on all predictor variables was available, ensuring consistency in the statistical analysis but limiting the useable dataset to 109 cases. Accordingly, the predictive model was intentionally designed around a small set of physically meaningful variables for which data were available in the literature, reducing the risk of spurious correlations and ensuring that the resulting model remains interpretable and robust despite the modest sample size.

5.1. Prediction model functional form

The functional form of a predictive model plays a crucial role in determining both the accuracy and reliability of regression analyses. Initially, predictive models in seismic engineering, such as ground motion prediction models, considered only earthquake parameters. However, subsequent studies demonstrated the importance of incorporating site-specific and structural parameters to account for local variability and the influence of different embankment characteristics. For instance Ref. [51], illustrated the process of selecting appropriate functional forms for ground motion equations in regions with sparse data, using the Himalayas as a case study. Similarly [52], highlighted that functional forms for intensity prediction differ from those for ground motion, and they developed an intensity predictive equation specifically for the Himalayan region. Given the absence of predictive models to predict dam damage intensity, we identify suitable functional forms to develop robust predictive equations for DDI. DDI predictive models were formulated by adapting functional forms from previously established Intensity Prediction Equations (IPEs) [52,53], Ground Motion Prediction Equations (GMPEs) [54], and a dam crest settlement model [55]. This resulted in four candidate predictive equations for DDI, expressed as follows:

1) *Model 1 (Log-Linear Form):* This model was modified from the dam crest settlement model given by Ref. [55].

$$DDI = \beta_1 + \beta_2 \log M + \beta_3 \log R + \beta_4 \log H_D + \beta_5 \log A_D + \beta_6 \log DT_1 + \beta_7 \log DT_2 \quad (1)$$

2) *Model 2 (Nonlinear Mixed Form):* This model was modified from a generalized GMPE form as discussed by Ref. [54].

$$DDI = \beta_1 + \beta_2 M + \beta_3 M^{\beta_4} + \beta_5 \log\left(R + \beta_6 e^{\beta_7 M}\right) + \beta_8 R + \beta_9 H_D + \beta_{10} A_D + \beta_{11} DT_1 + \beta_{12} DT_2 \quad (2)$$

3) *Model 3 (Linear-log Mixed Form):* This model was modified from an IPE form, as discussed by Ref. [53].

$$DDI = \beta_1 + \beta_2 M + \beta_3 \log R + \beta_4 R + \beta_5 H_D + \beta_6 A_D + \beta_7 DT_1 + \beta_8 DT_2 \quad (3)$$

4) *Model 4 (Quadratic-log Mixed Form):* This model was modified from an IPE form, as discussed by Ref. [52].

$$DDI = \beta_1 + \beta_2 M + \beta_3 M^2 + \beta_4 \log R + \beta_5 R + \beta_6 H_D + \beta_7 A_D + \beta_9 DT_1 + \beta_{10} DT_2 \quad (4)$$

in these models, β_i denotes regression coefficients, M represents the moment magnitude (M_w), R is the hypocentral distance (R_{hyp}), H_D is the dam height, A_D is the age of the dam, and DDI represents the dam damage intensity. R_{hyp} is calculated as:

$$R_{hyp} = \sqrt{R_{epi}^2 + D_f^2} \quad (5)$$

where R_{epi} denotes the epicentral distance and D_f the focal depth. All predictors in the four models were selected based on their physical or engineering relevance [52–55]. Earthquake magnitude (M, M^2, M^{β_4} terms) serves as the primary driver of seismic damage, with nonlinear or quadratic terms enabling flexible scaling of damage severity [52–55]. Hypocentral distance (R, $\log(R + \beta_6 e^{\beta_7 M})$ terms) accounts for geometric spreading and attenuation of seismic waves along the source-to-dam path, incorporating focal depth through R_{hyp} [52–55]. H_D reflects structural inertia and hydrodynamic forces that influence dam response, as well as stiffness is somewhat represented in H_D, accounting on seismic energy absorption and structural resilience, with taller dams generally presenting higher sliding and overturning risks [45–47]. A_D is used as an empirical proxy for cumulative, time-dependent effects such as settlement, cracking, and seepage changes; it does not imply a mechanistic deterioration rate or reduction in material strength. To capture the effect

of different types of embankment dams, the categorical variable DT was incorporated into the regression models. Three categories were identified: homogeneous dams, rockfill dams, and earth-cored dams. The earthen dam was designated as the baseline category, and two dummy variables were introduced:

$$DT = \begin{cases} Homogeneous\ dam : (DT_1, DT_2) = (0,0) \\ Rockfill\ dam : (DT_1, DT_2) = (1,0) \\ Earth\ cored\ dam : (DT_1, DT_2) = (0,1) \end{cases}$$

For the baseline (earthen dams), both dummy variables are zero, indicating that no categorical adjustment is applied in the regression model. These dummy variables were introduced as additive terms in the regression equations to quantify the influence of dam type on DDI. The intercept term (β_1), therefore, represents the expected DDI for earthen dams (baseline), while the coefficients associated with DT_1 and DT_2 capture the mean deviations in DDI for rockfill and earth-cored dams, respectively, relative to the baseline category. Although the indices of these coefficients differ among models due to differences in total parameter count, their interpretation remains consistent across all functional forms. Specifically, they act as constant additive offsets that modify the baseline prediction without altering the relationships between DDI and the primary explanatory variables (M, R, H_D, and A_D). This formulation provides a physically interpretable representation of categorical effects, treating dam-type influences as fixed offsets that preserve the functional form of the base model. The approach is analogous to the use of source-type constants in GMPEs [56], which capture systematic differences among crustal, interface, and intraslab events while maintaining a shared functional structure.

Two complementary modelling strategies were employed. In the combined analysis, all dam types were included simultaneously, allowing the model to capture dam-type-dependent variations related to magnitude, distance, height, and ageing. In the type-specific analysis, separate regressions were performed for each dam type independently (omitting DT terms). This dual strategy captures both inter-type and intra-type variability in dam response, ensuring robust and physically interpretable predictive relationships. Fig. 6 presents the correlation matrix of variables used in the models. The selection of the most suitable predictive model will be based on evaluation metrics, which are discussed in subsequent sections. This functional form framework ensures that seismic, structural, and ageing effects are systematically captured in the predictive modelling of dam damage intensity.

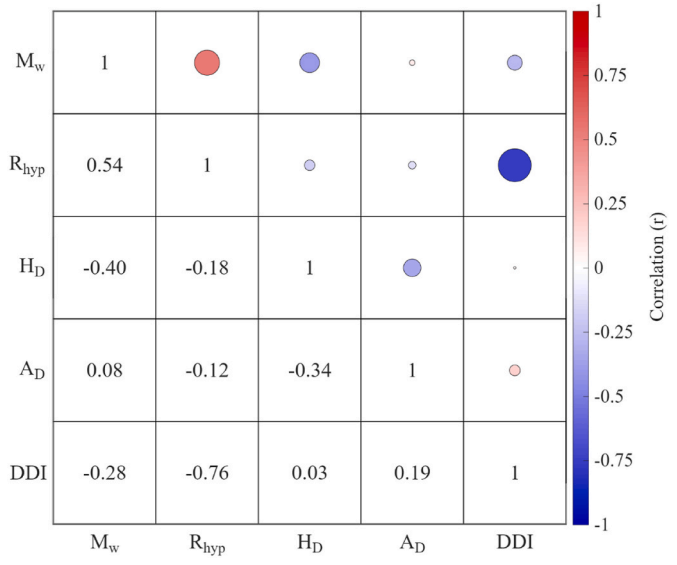

Fig. 6. Correlation matrix for the variables (Magnitude (M_w), Hypocentral Distance (R_{hyp}), Dam Height (H_D), Age of Dam (A_D), Dam Type (DT), Dam Damage Intensity (DDI)) used in the analysis.

6. Model evaluation parameters and selection criteria

DDI predictive models were systematically assessed using complementary residual-based and likelihood-based metrics. Together, these approaches provide a comprehensive understanding of model behaviour, including systematic bias, dispersion of predictions, error magnitude, and information-theoretic fit.

6.1. Residual-based evaluation metrics

Residual-based metrics quantify the differences between observed and predicted values, providing insight into both systematic errors and overall prediction accuracy. The key metrics applied in this study are summarised in Table 3.

6.2. Likelihood-based metric and model ranking

To complement conventional residual-based performance measures with an information-theoretic perspective, the average sample log-likelihood (LLH) was employed as a likelihood-based metric for model evaluation and ranking. The LLH quantifies the agreement between model-predicted and observed data distributions, assuming that the residuals follow a Gaussian distribution with standard deviation (σ). It is mathematically expressed as:

$$LLH = -\frac{1}{n}\sum_{i=1}^{n} log\left[\frac{1}{\sqrt{2\pi\sigma}} e^{\left(-\frac{(y_i-\hat{y}_i)^2}{2\sigma^2}\right)}\right] \quad (6)$$

where y_i and $\hat{y}_i$ denote the observed and predicted values, respectively, and n is the total number of samples. This formulation represents the negative mean log-probability of observing the data given the model and its uncertainty structure. Lower LLH values correspond to smaller information loss when the candidate model replaces the empirical distribution, and are therefore indicative of better model performance [63,64]. LLH metric integrates both model fit and uncertainty, offering a probabilistically consistent and sample-size-independent evaluation of model adequacy. By framing model performance within an information-theoretic context, LLH provides a rigorous basis for model selection and ranking, particularly when comparing models of differing complexity or functional form. This approach aligns with established practices in seismological and geotechnical modelling, where

Table 3
Parameters used for the evaluation of predictive models.

Evaluation Parameters	Formula	References
Bias	$Bias = \frac{1}{n}\sum_{i=1}^{n}(y_i - \hat{y}_i)$	[57]
Coefficient of determination	$R^2 = 1 - \frac{\sum(y_i-\hat{y}_i)^2}{\sum(y_i-\tilde{y}_i)^2}$	[58,59]
Adjusted R^2	$R^2_{adj} = 1 - \left(\frac{(1-R^2)(n-1)}{n-k-1}\right)$	[60]
Mean Square Error	$MSE = \frac{1}{n}\sum_{i=1}^{n}(y_i-\hat{y}_i)^2$	[58]
Root Mean Square Error	$RMSE = \sqrt{\frac{1}{n}\sum(y_i-\hat{y}_i)^2}$	[58]
Mean Absolute Error	$MAE = \frac{1}{n}\sum_{i=1}^{n}\lvert y_i-\hat{y}_i\rvert$	[58]
Mean Absolute Percentage Error	$MAPE = \frac{100}{n}\sum_{i=1}^{n}\left\lvert\frac{y_i-\hat{y}_i}{y_i}\right\rvert$	[61]
Symmetric Mean Absolute Percentage Error	$sMAPE = \frac{100}{n}\sum_{i=1}^{n}\frac{\lvert y_i-\hat{y}_i\rvert}{\frac{(\lvert y_i\rvert+\lvert\hat{y}_i\rvert)}{2}}$	[62]

Abbreviations: y: output DDI, y_i: actual observed values of y, $\hat{y}_i$: predicted y values from the model, n: number of observations, $\tilde{y}_i$: mean of y, k: number of independent variables.

likelihood-based criteria are widely used to identify the most plausible predictive relationships among competing formulations [63]. Accordingly, models exhibiting the lowest LLH values are interpreted as statistically superior, reflecting a higher likelihood of reproducing the observed data within the assumed uncertainty bounds.

6.3. Selection criteria and synthesis

Model selection proceeded in two stages. First, candidate models were ranked by LLH to identify those with the least information loss. Second, this likelihood-based ranking was cross-checked against residual-based metrics to verify that the LLH-optimal model also exhibited acceptable bias, low error magnitude, and consistent variance explanation. By combining these complementary perspectives, the final selected model was the one that minimised LLH while maintaining favourable residual statistics, thereby offering the strongest balance of explanatory power, predictive precision, and parsimony for subsequent analyses.

6.4. Predictive model validation

The predictive performance of the models was evaluated using repeated resampling-based internal validation, which is appropriate for small to moderate sample sizes and in situations where independent external test datasets are unavailable [65,66]. Two complementary approaches were applied: repeated stratified k-fold cross-validation [67] and non-parametric bootstrap resampling [68].

For repeated stratified k-fold cross-validation (CV), the dataset (N = 109) was divided into five approximately equal folds (k = 5). Stratification was performed using a combined index of discretised DDI bins and dam type to preserve both the response distribution and relevant categorical structure across folds. The 5-fold procedure was repeated 10 times with independent stratifications, resulting in a total of 50 out-of-sample evaluations. In each iteration, models were calibrated on four folds and evaluated on the held-out fold. Predictive performance was quantified using RMSE, MAE, and R^2, which were computed for each fold and summarised as mean ± standard deviation (SD) across all repetitions. Cross-validated predictions for all observations were retained and aggregated for subsequent diagnostic analyses, including residual inspection, observed–predicted relationships, and calibration assessment [67].

To quantify uncertainty in predictive performance, non-parametric bootstrap resampling (B = 1000) was applied to the paired observed values and the corresponding cross-validated predictions. Empirical 95 % confidence intervals for RMSE and MAE were derived from the resulting bootstrap distributions [68]. This procedure provides uncertainty-aware estimates of predictive accuracy while preserving the out-of-sample nature of the validation. The combined use of repeated cross-validation and bootstrap resampling enables a robust assessment of predictive accuracy, stability, and potential systematic bias under repeated sampling, while avoiding reliance on a single arbitrary data split. Although these resampling-based procedures do not replace validation on a truly independent external dataset, they provide a rigorous and transparent internal evaluation of predictive generalisability under the present data-limited conditions.

7. Results and discussions

7.1. Regression results

Predictive relationships for the DDI were calibrated by regressing the selected seismic and dam-related variables against the observed DDI values. The estimated coefficients for all candidate models are reported in Tables 4–7, encompassing both the combined embankment-dam dataset and the individual dam-type subsets. The resulting R^2 demonstrates the strong explanatory power of the predictor variables. The type-specific calibrations capture dam type-dependent behaviour, whereas the combined model reveals consistent patterns across the broader embankment dam. Scatter plots of predicted versus observed values (Fig. 7) further confirm that the calibrated models accurately reproduce the measured data, thereby demonstrating their adequacy in capturing the principal trends in the dataset.

Residuals were analysed to evaluate model adequacy and detect systematic errors. Residuals of the final selected model plotted against R_{hyp} are shown in Fig. 8. Residuals plotted against R_{hyp} exhibit a random scatter around zero with no discernible trend, suggesting homoscedasticity and the absence of distance-dependent bias. These results demonstrate the reliability of the predictive models across the observed DDI range.

Table 4
Regression coefficients of the predictive models for the combined data analysis (all Embankment dam types).

Parameters		Model1	Model2	Model3	Model4
Coefficients	β_1	−10.144	1.123	−3.017	−37.188
	β_2	10.513	−7.093	0.621	9.956
	β_3	−2.177	7.161	1.037	−0.631
	β_4	0.197	1.027	−0.036	0.997
	β_5	0.164	0.180	−0.006	−0.036
	β_6	0.287	0.661	0.007	−0.007
	β_7	0.076	0.166	−0.028	0.008
	β_8	–	−0.027	0.342	−0.079
	β_9	–	−0.005	–	0.219
	β_{10}	–	0.005	–	–
	β_{11}	–	−0.016	–	–
	β_{12}	–	0.183	–	–
Metrics	R^2	0.538	0.612	0.620	0.621
	Adjusted R^2	0.505	0.563	0.589	0.586
	RMSE	0.981	0.898	0.889	0.888

Table 5
Regression coefficients of predictive models for the CED.

Parameters		Model1	Model2	Model3	Model4
Coefficients	β_1	1.145	0.673	−0.520	4.115
	β_2	4.292	−4.635	0.560	−0.728
	β_3	−1.462	5.023	0.412	0.088
	β_4	−0.299	1.013	−0.023	0.424
	β_5	0.143	0.059	−0.019	−0.023
	β_6	–	0.766	0.011	−0.019
	β_7	–	0.966	–	0.011
	β_8	–	−0.018	–	–
	β_9	–	−0.017	–	–
	β_{10}	–	0.010	–	–
	β_{11}	–	–		
Metrics	R^2	0.630	0.701	0.703	0.703
	Adjusted R^2	0.550	0.534	0.623	0.605
	RMSE	0.930	0.837	0.833	0.833

Table 6
Regression coefficients of the predictive models for the RCD.

Parameters		Model1	Model2	Model3	Model4
Coefficients	β_1	2.420	−11.874	−17.637	−1411.530
	β_2	5.748	0.556	0.524	362.169
	β_3	−2.717	−33100.787	5.070	−23.437
	β_4	0.147	−7.438	−0.070	5.258
	β_5	0.231	3.492	0.001	−0.073
	β_6	–	0.634	0.007	−0.022
	β_7	–	−0.651	–	0.013
	β_8	–	−0.057	–	–
	β_9	–	0.000	–	–
	β_{10}	–	0.005	–	–
	β_{11}	–	–	–	–
Metrics	R^2	0.427	0.434	0.435	0.611
	Adjusted R^2	0.290	0.080	0.265	0.468
	RMSE	0.957	0.952	0.951	0.789

Table 7
Regression coefficients of the predictive models for the HED.

Parameters		Model1	Model2	Model3	Model4
Coefficients	β_1	6.740	0.929	1.437	0.991
	β_2	12.936	0.430	4.497	0.932
	β_3	−6.412	0.654	−7.338	0.453
	β_4	0.069	0.340	0.007	−7.338
	β_5	0.035	0.349	0.007	0.007
	β_6	–	1.032	−0.001	0.007
	β_7	–	1.233	–	−0.001
	β_8	–	−0.050	–	–
	β_9	–	0.003	–	–
	β_{10}	–	0.003	–	–
	β_{11}	–	–	–	–
Metrics	R^2	0.805	0.796	0.805	0.805
	Adjusted R^2	0.783	0.745	0.779	0.774
	RMSE	0.573	0.586	0.573	0.573

7.2. Model selection and performance discussion

Final model selection was guided by both LLH and residual-based metrics to balance predictive accuracy, parsimony, and explanatory power. From Table 8, we can see that across the combined dataset analysis, Models 3 and 4 consistently outperformed the other candidates, achieving the highest R^2 (0.6197–0.6210) and adjusted R^2 (0.5858–0.5886) values, alongside the lowest MSE, RMSE, MAE, MAPE, and sMAPE, indicating superior predictive capability. LLH results corroborate these findings, with the lowest scores (1.3001–1.3018) reflecting minimal information loss. Dam type-specific analyses showed similar patterns: for HED, Models 3 and 4 attained $R^2 \approx 0.805$ with the lowest errors; in RFD, Model 4 achieved the highest R^2 (0.6112) and lowest error measures; and for CED, Models 3 and 4 maintained $R^2 \approx 0.703$ with consistently low error metrics, demonstrating robustness across dam types.

Predicted DDI values (Fig. 9) indicate that Models 1 and 2 produce conservative estimates, whereas Models 3 and 4 yield higher, more responsive predictions. Such sensitivity is advantageous in seismic damage assessment, where underestimation may compromise preparedness and increase risk [69], while overestimation, though potentially resource-intensive, generally ensures system protection [70]. Accordingly, Models 3 and 4 are recommended for predictive applications due to their superior accuracy, robustness, and reliability across dam types.

7.3. Predictive model validation discussion

The out-of-sample validation results reveal consistent and systematic differences in predictive accuracy and stability among the four candidate models. Across repeated stratified cross-validation and bootstrap uncertainty analysis, Models 3 and 4 consistently outperform Models 1 and 2, while Model 2 exhibits unstable and non-generalizable behaviour. The results of the repeated stratified 5-fold cross-validation (10 repetitions) are summarised in Table 9. Model 3 achieves the lowest CV RMSE (0.95002 ± 0.01370) and lowest CV MAE (0.78993 ± 0.00894), followed by Model 4 (CV RMSE = 0.97261 ± 0.02273). Model 1 shows moderate predictive performance, whereas Model 2 exhibits substantially larger variability (CV RMSE SD = 0.38794; CV R^2 = 0.042 ± 1.464), indicating weak and unstable generalisation.

These quantitative results are visually supported by the cross-validation scatter and residual plots (Figs. 10 and 11). In Fig. 10,

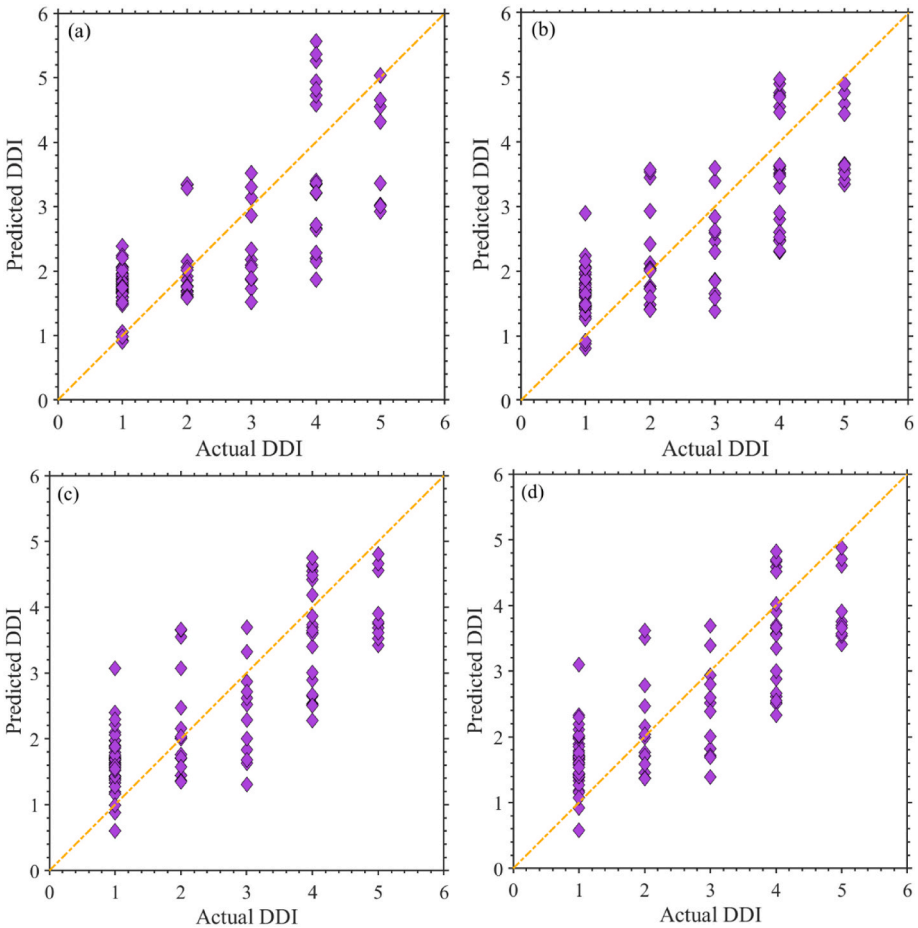

Fig. 7. Predicted DDI variation with actual DDI for the combined analysis, a) Model 1; b) Model 2; c) Model 3; d) Model 4.

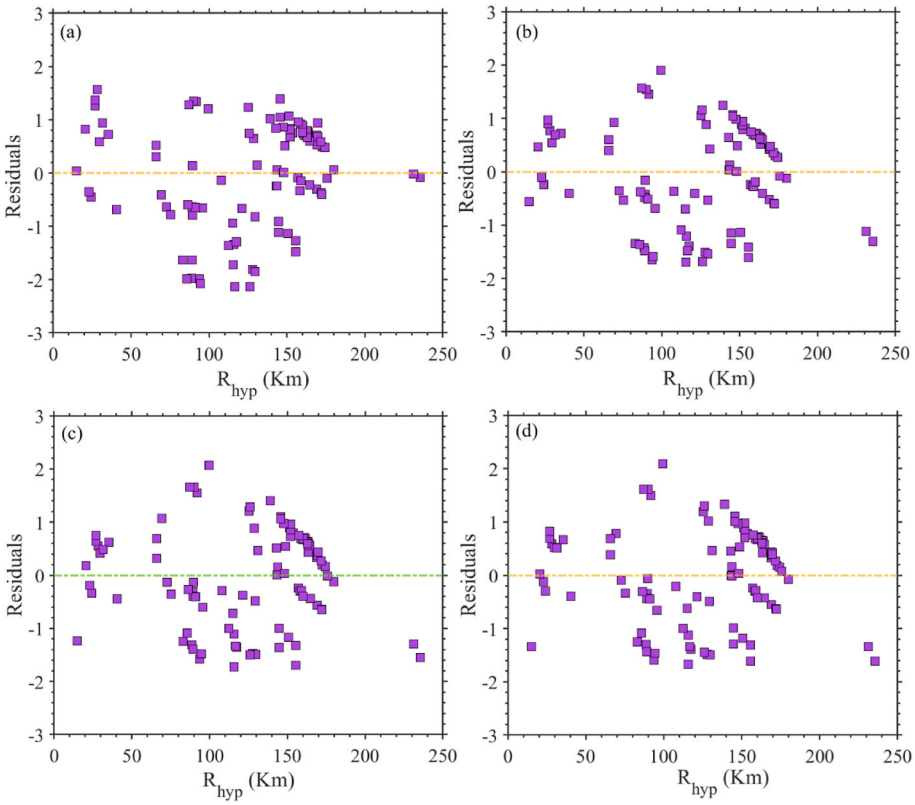

Fig. 8. Residuals plotted against hypocentral distance (R_{hyp}) for the four regression models: (a) Model 1; (b) Model 2; (c) Model 3; (d) Model 4.

Table 8
Performance matrices of all four models for the combined and individual dam-type data analyses.

Dam Type	Model	Bias	R^2	Adj R^2	MSE	RMSE	MAE	MAPE	sMAPE	LLH
All	Model1	0.000	0.538	0.505	0.962	0.981	0.835	44.748	37.745	1.399
	Model2	0.001	0.612	0.563	0.806	0.898	0.773	43.526	38.344	1.311
	Model3	0.000	0.620	0.589	0.791	0.889	0.750	43.142	37.415	1.302
	Model4	0.000	0.621	0.586	0.788	0.888	0.748	43.099	37.249	1.300
HED	Model1	0.000	0.805	0.783	0.329	0.573	0.452	29.378	26.990	0.863
	Model2	0.000	0.796	0.745	0.343	0.586	0.468	31.798	29.219	0.884
	Model3	0.000	0.805	0.779	0.328	0.573	0.450	29.033	26.739	0.862
	Model4	0.000	0.805	0.774	0.328	0.573	0.450	29.033	26.739	0.862
RFD	Model1	0.000	0.427	0.290	0.917	0.957	0.853	40.766	35.192	1.376
	Model2	0.003	0.434	0.080	0.906	0.952	0.817	39.985	33.982	1.370
	Model3	0.000	0.435	0.265	0.904	0.951	0.810	39.821	33.726	1.369
	Model4	0.000	0.611	0.468	0.622	0.789	0.646	28.169	25.639	1.182
CED	Model1	0.000	0.630	0.550	0.866	0.930	0.778	40.328	33.260	1.347
	Model2	0.000	0.700	0.534	0.701	0.837	0.678	34.670	27.910	1.242
	Model3	0.000	0.703	0.623	0.694	0.833	0.663	34.827	27.694	1.237
	Model4	0.000	0.703	0.605	0.694	0.833	0.662	34.732	27.605	1.237

Model 3 exhibits the tightest clustering around the 1:1 reference line, indicating the highest predictive accuracy and minimal systematic bias. Model 4 follows closely with only slightly greater dispersion. Model 1 displays visibly larger scatter and deviations at the extreme values, while Model 2 shows substantial dispersion and weak alignment with the 1:1 line, confirming poor generalisation. The residual plots in Fig. 11 further reinforce these trends: residuals of Models 3 and 4 are symmetrically distributed around zero with no pronounced heteroscedasticity, whereas Model 1 shows larger residual amplitudes and Model 2 exhibits wide residual spread, outliers, and non-random structure indicative of numerical instability.

Fig. 12 compares the distribution of predictive errors for all candidate models under repeated cross-validation. Model 3 consistently achieves the lowest median RMSE and the narrowest interquartile range, indicating both superior predictive accuracy and robustness. Model 4 performs comparably but with slightly higher medians and wider spreads, while Model 1 occupies an intermediate position. In contrast, Model 2 exhibits a markedly wider error distribution with numerous outliers and heavy-tailed behaviour, confirming pronounced instability and unreliable predictive performance.

Bootstrap resampling of cross-validated predictions (B = 1000) provides uncertainty-aware estimates of prediction error (Table 10). Model 3 exhibits the lowest RMSE and MAE together with the narrowest 95 % confidence intervals, confirming superior robustness. Model 4 also shows relatively narrow intervals but remains slightly inferior to Model 3. Model 2 displays the widest uncertainty bounds, further indicating limited predictive reliability.

The out-of-sample validation results are fully consistent with the training-based goodness-of-fit and log-likelihood (LLH) evaluation presented in Table 8. Models 3 and 4 previously achieved the highest R^2

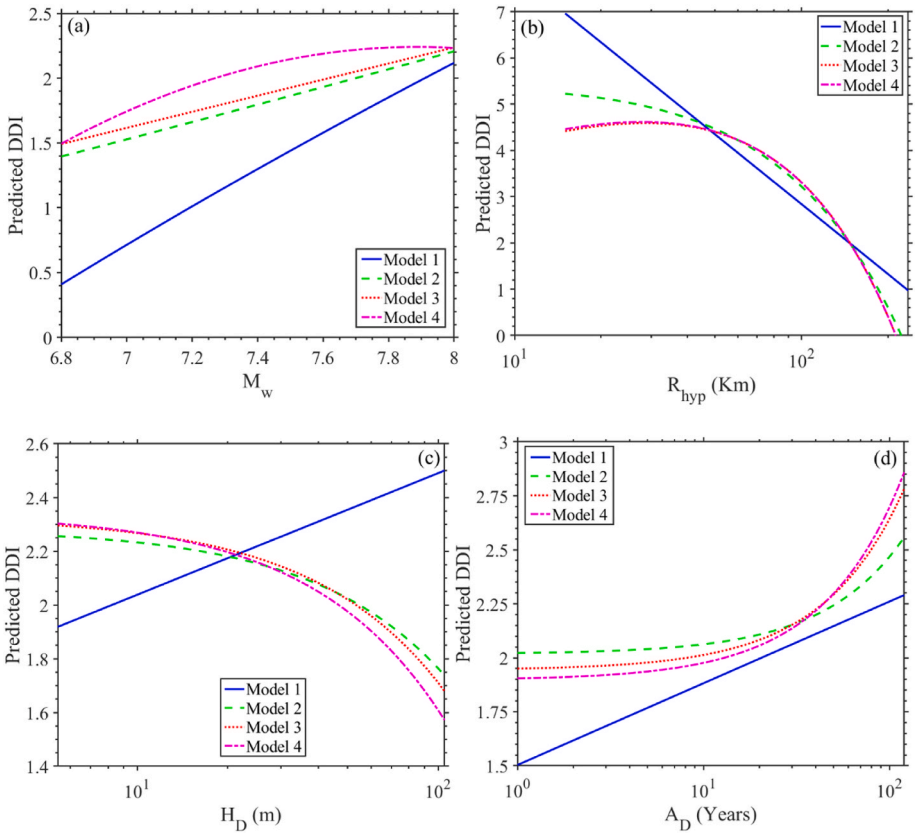

Fig. 9. Variation of DDI with respect to each independent variable: a) Magnitude (M_w); b) Height of dam (H_D); c) Age of dam (A_D); d) Hypocentral distance (R_{hyp}).

Table 9
Repeated stratified 5-fold cross-validation results (mean ± SD).

Model	CV RMSE (mean ± SD)	CV MAE (mean ± SD)	CV R^2 (mean ± SD)
Model 1	1.02310 ± 0.01288	0.87275 ± 0.01041	0.493 ± 0.012
Model 2	1.11080 ± 0.38794	0.92611 ± 0.29310	0.042 ± 1.464
Model 3	0.95002 ± 0.01370	0.78993 ± 0.00894	0.562 ± 0.012
Model 4	0.97261 ± 0.02273	0.80724 ± 0.01903	0.539 ± 0.021

(0.6197–0.6210) and adjusted R^2 (0.5858–0.5886), together with the lowest MSE, RMSE, MAE, MAPE, and sMAPE, and the lowest LLH values (1.3001–1.3018). The agreement between in-sample and cross-validated out-of-sample rankings indicates that the superior performance of Models 3 and 4 is not driven by overfitting.

Based on the combined evidence from repeated cross-validation (Table 9), bootstrap uncertainty analysis (Table 10), residual diagnostics, and training-based goodness-of-fit and LLH metrics (Table 8), Model 3 is selected as the final predictive model, with Model 4 identified as a secondary alternative. The unstable behaviour of Model 2 precludes its use for predictive applications. Overall, the consistency between likelihood-based in-sample metrics and resampling-based out-of-sample validation provides strong statistical support for the robustness and predictive generalisability of the selected model under data-limited conditions. Although these internal validation procedures do not substitute for validation on a truly independent external dataset, they provide a rigorous and transparent internal assessment of predictive generalisability for the present study.

7.4. Recommended DDI predictive model equations

Based on the calibration, residual, likelihood analyses, and out-of-sample validation results, the final recommended predictive equations for DDI are presented below, along with their corresponding applicability ranges:

1) For all types of Embankment dams:

$$DDI = -3.017 + 0.621M + 1.037 \log R - 0.036\,R - 0.006H_D + 0.007A_D - 0.028\,DT_1 - 0.342DT_2 \quad (7)$$

$$DDI = -37.19 + 9.96\,M - 0.63\,M^2 + 0.997 \log R - 0.04R - 0.007H_D + 0.008A_D - 0.08DT_1 - 0.22DT_2 \quad (8)$$

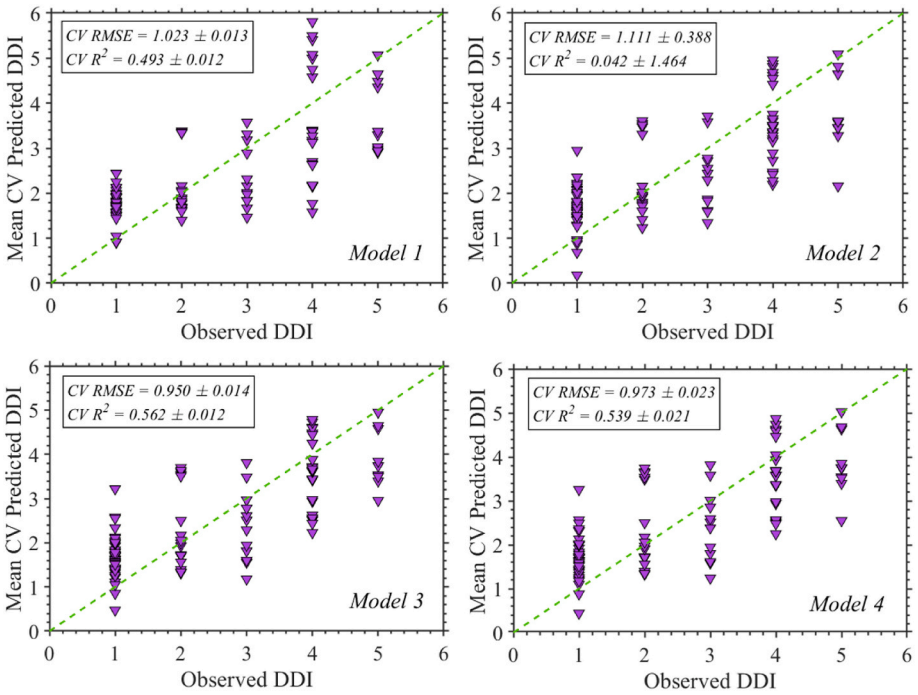

Fig. 10. Cross-validated observed versus mean predicted dam damage intensity (DDI) for all four models. Points represent out-of-sample predictions obtained from repeated stratified 5-fold cross-validation (10 repetitions), with predictions averaged across repeats. The dashed line denotes the 1:1 reference for perfect agreement.

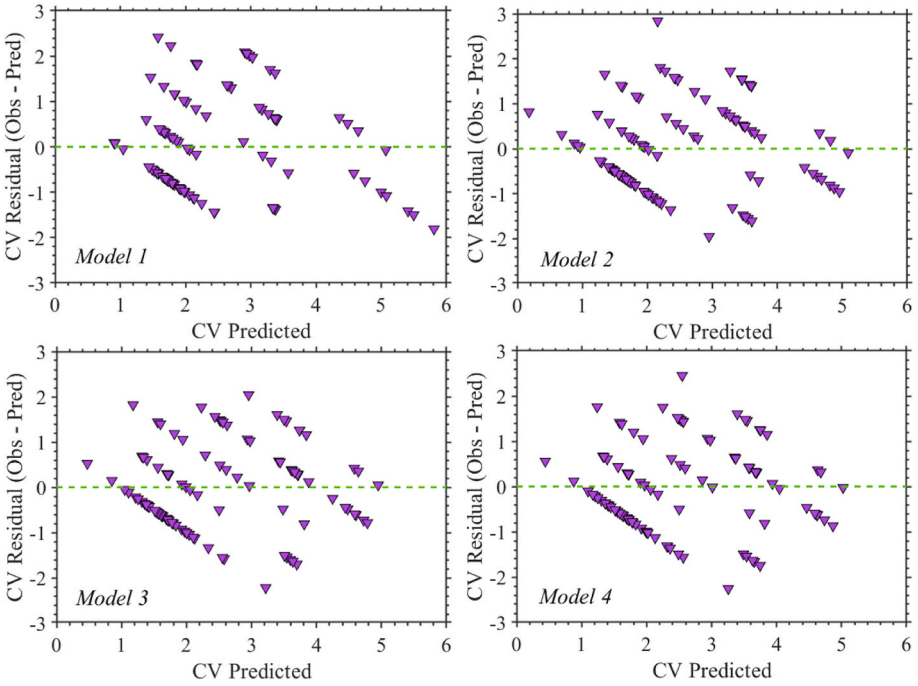

Fig. 11. Cross-validated residuals versus cross-validated predicted dam damage intensity (DDI) for all four models. Residuals are computed as observed minus predicted values from repeated stratified 5-fold cross-validation (10 repetitions), with predictions averaged across repeats. The dashed horizontal line denotes zero residual.

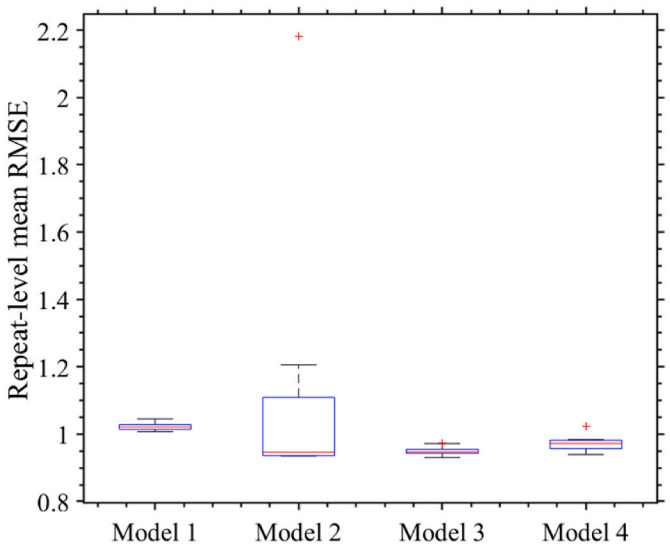

Fig. 12. Distribution of prediction errors for all candidate models based on repeated stratified 5-fold cross-validation (10 repetitions). Boxes represent the interquartile range (IQR), the central line denotes the median, whiskers indicate 1.5 × IQR, and red crosses denote outliers.

Table 10
Bootstrap 95 % confidence intervals for RMSE and MAE based on cross-validated predictions.

Model	CV RMSE	CV RMSE 95 % CI	CV MAE	CV MAE 95 % CI
Model 1	1.02310	0.89836–1.12570	0.87275	0.75247–0.97121
Model 2	1.11080	0.84205–1.07130	0.92611	0.70496–0.90471
Model 3	0.95002	0.83994–1.04770	0.78993	0.68580–0.88460
Model 4	0.97261	0.86116–1.08120	0.80724	0.69388–0.90796

$$\text{Constraints} = \begin{cases} \mathrm{M} = 8, \mathrm{M} \text{ is Moment magnitude } (\mathrm{M_w}) \\ 82 \le \mathrm{R} \le 175, \mathrm{R} \text{ is Hypocentral distance } (\mathrm{R_{hyp}}) \text{ in km} \\ 6 \le \mathrm{H_D} \le 47, \mathrm{H_D} \text{ is Height of Dam in m} \\ 17 \le \mathrm{A_D} \le 55, \mathrm{A_D} \text{ is Age of dam in years} \end{cases}$$

3) For the RFD:

$$\mathrm{DDI} = -17.637 + 0.524\mathrm{M} + 5.070 \log \mathrm{R} - 0.069\mathrm{R} + 0.001\,\mathrm{H_D} + 0.007\mathrm{A_D} \tag{11}$$

$$\mathrm{DDI} = -1411.530 + 362.169\mathrm{M} - 23.437\mathrm{M}^2 + 5.258 \log \mathrm{R} - 0.073\mathrm{R} - 0.022\mathrm{H_D} + 0.013\mathrm{A_D} \tag{12}$$

$$\text{Constraints} = \begin{cases} 6 \le \mathrm{M} \le 8, \mathrm{M} \text{ is Moment magnitude } (\mathrm{M_w}) \\ 15 \le \mathrm{R} \le 234, \mathrm{R} \text{ is Hypocentral distance } (\mathrm{R_{hyp}}) \text{ in km} \\ 5 \le \mathrm{H_D} \le 105, \mathrm{H_D} \text{ is Height of Dam in m} \\ 1 \le \mathrm{A_D} \le 120, \mathrm{A_D} \text{ is Age of dam in years} \\ (\mathrm{DT_1}, \mathrm{DT_2}) \in \{(0,0),(1,0),(0,1)\}, \begin{cases} (0,0) : \text{HED} \\ (1,0) : \text{RFD} \\ (0,1) : \text{CED} \end{cases} \end{cases}$$

$$\text{Constraints} = \begin{cases} 7 \le \mathrm{M} \le 8, \mathrm{M} \text{ is Moment magnitude } (\mathrm{M_w}) \\ 65 \le \mathrm{R} \le 170, \mathrm{R} \text{ is Hypocentral distance } (\mathrm{R_{hyp}}) \text{ in km} \\ 5 \le \mathrm{H_D} \le 105, \mathrm{H_D} \text{ is Height of Dam in m} \\ 1 \le \mathrm{A_D} \le 56, \mathrm{A_D} \text{ is Age of dam in years} \end{cases}$$

4) For the CED:

$$\mathrm{DDI} = -0.520 + 0.560\mathrm{M} + 0.412 \log \mathrm{R} - 0.023\mathrm{R} - 0.019\,\mathrm{H_D} + 0.011\mathrm{A_D} \tag{13}$$

$$\mathrm{DDI} = 4.115 - 0.728\,\mathrm{M} + 0.088\,\mathrm{M}^2 + 0.424 \log \mathrm{R} - 0.023\,\mathrm{R} - 0.019\,\mathrm{H_D} + 0.011\mathrm{A_D} \tag{14}$$

2) For the HED:

$$\mathrm{DDI} = 1.437 + 4.497\mathrm{M} - 7.338 \log \mathrm{R} + 0.007\,\mathrm{R} + 0.007\,\mathrm{H_D} - 0.001\mathrm{A_D} \tag{9}$$

$$\text{Constraints} = \begin{cases} 6 \le \mathrm{M} \le 8, \mathrm{M} \text{ is Moment magnitude } (\mathrm{M_w}) \\ 15 \le \mathrm{R} \le 236, \mathrm{R} \text{ is Hypocentral distance } (\mathrm{R_{hyp}}) \text{in km} \\ 9 \le \mathrm{H_D} \le 95, \mathrm{H_D} \text{ is Height of Dam in m} \\ 2 \le \mathrm{A_D} \le 120, \mathrm{A_D} \text{ is Age of dam in years} \end{cases}$$

$$\mathrm{DDI} = 0.991 + 0.932\mathrm{M} + 0.453\mathrm{M}^2 - 7.338 \log \mathrm{R} + 0.007\mathrm{R} + 0.007\mathrm{H_D} - 0.001\mathrm{A_D} \tag{10}$$

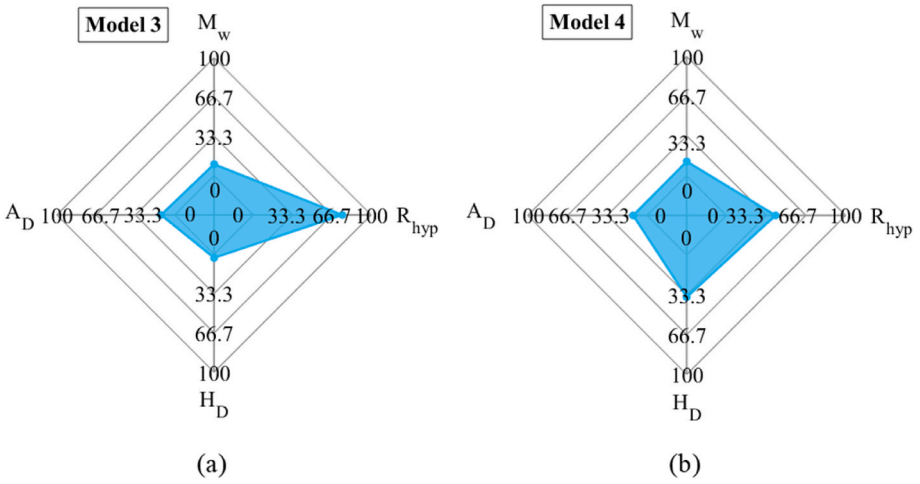

Fig. 13. Relative contribution of each predictor variable (Magnitude (M_w), Hypocentral Distance (R_{hyp}), Dam Height (H_D), Age of Dam (A_D)) to DDI predictions for rockfill dams: (a) Model 3; (b) Model 4.

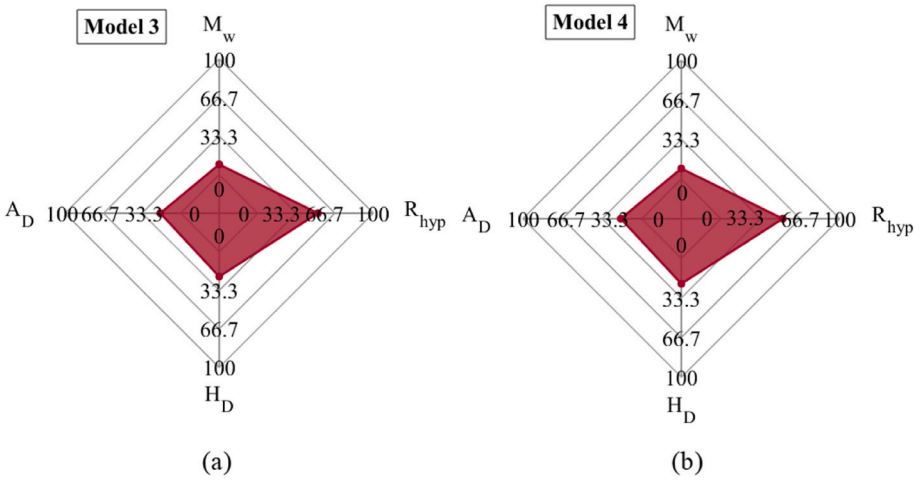

Fig. 14. Relative contribution of each predictor variable (Magnitude (M_w), Hypocentral Distance (R_{hyp}), Dam Height (H_D), Age of Dam (A_D)) to DDI predictions for earth core dams: (a) Model 3; (b) Model 4.

For operational use, it is important to note that DDI is typically reported in discrete intensity levels. Therefore, predicted DDI values that are not natural numbers should be rounded to the nearest integer [71]. For example, a predicted value of 1.5 would be rounded to 2. Additionally, these predictive equations are valid only within the ranges of independent variables used for model calibration. Extrapolation beyond these ranges may reduce predictive accuracy. By following these guidelines, Eqs. (7)–(14) can be effectively used to estimate DDI across a variety of dam types and seismic scenarios, providing a robust tool for risk assessment and decision-making.

7.5. *Relative contribution of predictor variables in DDI predictions*

The relative importance of the predictor variables A_D, H_D, R_{hyp}, and M_w was analysed for the top-performing DDI models (Models 3 and 4) of each dam type (rockfill and earth-cored). The homogeneous earthen dam type was excluded from this analysis due to limited variability in M_w, as all data corresponded to a single earthquake magnitude. A sensitivity analysis was used to quantify the relative contributions of each predictor variable to the DDI. Each variable was varied systematically across its observed range while the others were held constant at their mean values. The effects were normalised to percentage contributions following the procedure outlined in previous studies [72–74].

For rockfill dams in Model 3 (Fig. 13a), the DDI predictions were strongly dominated by the R_{hyp}, which contributed 75.54 % of the total influence. The remaining variables exhibited comparatively minor contributions, with A_D at 11.64 %, M_w at 9.73 %, and H_D at 3.08 %. In Model 4 (Fig. 13b), however, the relative contribution pattern became more balanced. The influence of R_{hyp} decreased to 41.19 %, while the contribution of H_D increased substantially to 35.25 %, indicating that dam height becomes a critical factor in determining seismic response as model complexity improves. The contributions of M_w (11.97 %) and A_D (11.60 %) were also comparable, suggesting a more integrated influence of both seismic and structural parameters. For earth-cored dams, the relative contributions of predictor variables were more evenly distributed across both Model 3 (Fig. 14a) and Model 4 (Fig. 14b). In both models, R_{hyp} remained the most influential parameter, contributing approximately 52 % to DDI prediction. The H_D accounted for around 21 %, followed by A_D with 17.6 %, and M_w with approximately 9 %. These findings reinforce that the R_{hyp} is the primary earthquake-related parameter influencing DDI, while the H_D serves as the primary structural parameter influencing DDI predictions most. The A_D and M_w provide secondary modulation, reflecting the effects of structural mass and input energy, respectively.

7.6. Application and practical significance of the DDI scale and predictive model

The DDI scale and its associated predictive models provide a screening-level, data-driven, semi-empirical framework for preliminary seismic damage assessment and portfolio-level risk screening of embankment dams. The framework is not intended to replace detailed numerical analyses of dam behaviour, but rather to complement them by supporting early-stage decision-making and prioritisation. High-fidelity numerical approaches, such as nonlinear dynamic finite-element simulations of cracking, permanent displacements, and slope instability, require extensive site-specific inputs, including material properties, foundation conditions, and frequency-dependent ground-motion characterisation, as well as substantial computational resources. As a result, such methods are impractical as first-stage tools for large dam inventories or regional-scale hazard assessments [75]. For example, following an earthquake affecting a region, the DDI framework can be applied to rapidly screen a portfolio of dams and prioritise those requiring immediate detailed assessment.

In contrast, the DDI framework employs readily available and widely reported parameters (moment magnitude, hypocentral distance, dam height, age, and dam type) to generate consistent empirical indicators of expected damage severity. This enables rapid, transparent, and internally consistent ranking and prioritisation of embankment dams across regional or national portfolios, consistent with established risk-index approaches in dam safety practice [75]. The DDI therefore supports comparative assessment under conditions where detailed geotechnical and seismic information is unavailable or incomplete. By translating historical and post-earthquake qualitative observations (e.g., crack dimensions, leakage severity, deformation indicators, and post-event operability) into a structured damage-intensity scale, the DDI enables the systematic integration of legacy case histories into modern seismic risk-screening workflows. This capability is not directly achievable through purely numerical displacement-based analyses and provides a means of leveraging existing observational evidence within a consistent assessment framework.

Accordingly, the DDI fits within a two-tier seismic risk assessment paradigm, in which an initial screening-level DDI-based evaluation is used to identify and prioritise potentially vulnerable dams, followed by targeted site-specific geotechnical and seismic analyses for those identified as high risk (i.e., higher DDI levels). Such a workflow enhances the transparency, consistency, and cost-effectiveness of seismic safety evaluations and aligns with internationally recommended dam-safety protocols [49,75].

8. Summary and Conclusions

This study analysed historical cases of earthquake-induced damage to embankment dams, evaluated the effectiveness of the MMI scale to effectively classify the damage, and addressed the lack of dedicated seismic dam damage classification methods. The MMI scale was found to be limited in reliably classifying dam-specific earthquake damage, motivating the development of a novel seismic Dam Damage Intensity (DDI) scale. The DDI classifies seismic dam damage into five levels, defined by specific damage descriptions, dam characteristics, and post-earthquake usability. Scale was developed using data from approximately 109 dams affected by 16 earthquakes, integrating both seismic and dam-specific parameters to provide a more comprehensive assessment of potential damage severity. Due to the lack of predictive models, DDI predictive models were developed using modified functional forms of Intensity Prediction Equations (Models 3 & 4), Ground Motion Prediction Equations (Model 2), and Dam Crest Settlement Models (Model 1), incorporating both seismic and dam parameters. The contribution of the predictor variables in DDI prediction was also studied through sensitivity analysis. The key findings indicate that:

1) There is a notable absence of dedicated methodologies or scales for classifying seismic damage to embankment dams. The MMI scale, in particular, has limitations in effectively classifying seismic dam damage, which has led to the creation of a novel seismic damage classification known as the seismic DDI scale for more accurate dam damage assessments.
2) Analysis of the compiled dataset indicates that reported seismic damage to embankment dams is associated with earthquakes of magnitude approximately $M_w \geq 6.0$ occurring within hypocentral distances $R_{hyp} \leq 250$ km. These values reflect characteristics of the available historical records rather than universal damage thresholds.
3) All models were evaluated using residual-based metrics and LLH to balance predictive accuracy, parsimony, and explanatory power. Intensity Predictive Equation (IPE) functional form-based models (Models 3 and 4) consistently outperformed the others, achieving the highest R^2 and adjusted R^2, the lowest error metrics (MSE, RMSE, MAE, MAPE, sMAPE), and the lowest LLH (1.300–1.302) for the combined dataset, indicating strong predictive capability and minimal information loss.
4) DDI models for earthen dams showed $R^2 \approx 0.805$ and LLH $\approx$0.862 for Models 3 and 4; for rockfill dams, Model 4 attained $R^2 = 0.611$ and LLH $\approx$1.182; for earth-cored dams, Models 3 and 4 reached $R^2 \approx 0.703$ and LLH $\approx$1.237. These results confirm the robustness of IPE-based models (Models 3 and 4) across dam types.
5) Out-of-sample validation using repeated stratified cross-validation and bootstrap uncertainty showed that the IPE-based models (Models 3 and 4) consistently exhibited the strongest predictive performance. Model 3 achieved the lowest cross-validated RMSE (0.950 ± 0.014) and MAE (0.790 ± 0.009), followed closely by Model 4 (CV RMSE $= 0.973 \pm 0.023$; CV MAE $= 0.807 \pm 0.019$). Bootstrap analysis confirms the robustness of both IPE-based models, with Model 3 exhibiting narrow 95 % confidence intervals for RMSE (0.840–1.048) and MAE (0.686–0.885), and Model 4 showing comparably constrained uncertainty ranges.
6) Sensitivity analysis showed that R_{hyp} is the most influential seismic factor controlling DDI, followed by M_w. Among dam parameters, H_D was found to be the most influential factor, followed by A_D, indicating its stronger role in seismic response. H_D refers to the total dam height, not the height of the damaged section. Availability of more detailed dam-specific data may alter these contributions.

In conclusion, the DDI scale and predictive models offer a reliable tool for preliminary damage assessment for embankment dams in earthquake-prone regions. These results highlight the importance of integrating both seismic and structural characteristics for accurate vulnerability assessment.

9. Limitations and future research needs

This study has two main limitations: first, the relatively small sample size may restrict the generalisability of the findings. Expanding the dataset to include a broader range of dams across different regions and geological conditions would provide more robust insights wherever available. Second, while shear wave velocity (Vs) is recognised as an important parameter for assessing material stiffness and dynamic response, reliable site-specific Vs measurements were not available for the site and dam. For this reason, Vs was not included in the final models. Future research should aim to incorporate measured Vs values whenever available, as this could strengthen model accuracy and practical applicability. A further important limitation is the absence of a truly independent external validation dataset. While the employed internal resampling strategies provide a rigorous assessment of predictive stability under data-limited conditions, they cannot fully substitute for validation against independent post-event observations. Future research should therefore seek to test the proposed DDI models on externally sourced datasets as they become available. DDI models can include more detailed site-specific geotechnical and seismological parameters when

such data become available in future datasets. In addition, future work may also benefit from the use of larger datasets and advanced damage prediction techniques, such as machine learning.

CRediT authorship contribution statement

P. Anbazhagan: Writing – review & editing, Validation, Supervision, Funding acquisition, Conceptualization. **Surya Prakash:** Writing – review & editing, Writing – original draft, Visualization, Validation, Software, Methodology, Investigation, Formal analysis, Data curation, Conceptualization.

Declaration of Competing Interest

The authors declare that they have no known competing financial interests or personal relationships that could have appeared to influence the work reported in this paper.

Acknowledgment

The authors would like to thank the Dam Safety (Rehabilitation) Directorate, Central Water Commission, for funding the "International Centre of Excellence in Dam Engineering" (ICED) under the Dam Rehabilitation and Improvement Project (DRIP); Ministry of Jal Shakti (MoJS), Government of India for the project entitled "Integrated Investigation for Risk Assessment of the Dam" under grant R-24011/57/2023-Pen Riv Section-MOWR.

Appendix A. Supplementary data

Supplementary data to this article can be found online at https://doi.org/10.1016/j.soildyn.2025.110079.

Data availability

The dataset supporting this study is provided as supplementary material (Table S_1) associated with this article and can be found in Appendix A.

References

[1] Narita K. Design and construction of embankment dams. Dept. of civil eng. Aichi Institute of Technology; 2000.
[2] Fell R. Geotechnical engineering of dams. CRC press; 2005.
[3] Merchán-Sanmartín B, Aucapeña-Parrales J, Alcívar-Redrován R, Carrión-Mero P, Jaya-Montalvo M, Arias-Hidalgo M. Earth dam design for drinking water management and flood control: a case study. Water 2022;14(13):2029.
[4] Duncan JM, Wright SG, Brandon TL. Soil strength and slope stability. John Wiley & Sons; 2014.
[5] Tosun H. Earthquakes and dams. In: Earthquake engineering-from engineering seismology to optimal seismic design of engineering structures. IntechOpen; 2015.
[6] Tani S. Damage to earth dams. Soils Found 1996;36(Special):263–72.
[7] Ghiasi V, Azami M. Earth dam behavior under earthquake Movements-An overview. Reliabil Eng Resil 2022;4(1):1–30.
[8] Swaisgood JR. Embankment dam deformations caused by earthquakes. Pacific conference on earthquake engineering, vol. 14; 2003, February.
[9] Noguera Guillermo. Dam performance during the cauquenes (Chile) earthquake 27/02/2010. Hanoi, Vietnam: ' presentation to ICOLD Committee on Seismic Aspects of Dam Design; 2010. [Accessed 24 May 2010].
[10] Verdugo R, Sitar N, Frost JD, Bray JD, Candia G, Eldridge T, Urzua A. Seismic performance of earth structures during the February 2010 Maule, Chile, earthquake: dams, levees, tailings dams, and retaining walls. Earthq Spectra 2012;28(1_suppl1):75–96.
[11] Seed HB, Lee KL, Idriss IM, Makdisi F. Analysis of the slides in the San Fernando dams during the earthquake of Feb. 9, 1971. Coll Eng Univ California 1973;73(2).
[12] Abbas M, Takada S, Sepand S. Fujinuma dam performance during the 2011 Tohoku earthquake, Japan, and failure mechanism by FEM. The 15th world conference on earthquake engineering, vol. 15. Lisboa: WCEE; 2012.
[13] Hariri-Ardebili MA, Tosun H. Dams in the wake-up call of the 2023 Türkiye earthquake sequence: insights from observed damages, risk assessment, and monitoring. Int J Disaster Risk Reduct 2024;102:104284.
[14] Wood H, Neumann F. The Modified Mercalli intensity scale of 1931. Bull Seismol Soc Am 1931;21(4):277–83.
[15] Grünthal G. European macroseismic scale 1998 (EMS-98). 1998.
[16] Akkar S, Ilki A, Goksu C, Erdik M. Advances in assessment and modeling of earthquake loss. Springer Nature; 2021. p. 308.
[17] Dowrick DJ. The modified mercalli earthquake intensity scale: revisions arising from recent studies of New Zealand earthquakes. Bull N Z Soc Earthq Eng 1996;29(2):92–106.
[18] Anbazhagan P, Srinivas S, Chandran D. Classification of road damage due to earthquakes. Nat Hazards 2012;60:425–60.
[19] Mahboubi S, Shiravand MR. Seismic evaluation of bridge bearings based on damage index. Bull Earthq Eng 2019;17:4269–97.
[20] Rosti A, Rota M, Penna A. Damage classification and derivation of damage probability matrices from L'Aquila (2009) post-earthquake survey data. Bull Earthq Eng 2018;16:3687–720.
[21] Polese M, d'Aragona MG, Prota A. Simplified approach for building inventory and seismic damage assessment at the territorial scale: an application for a town in southern Italy. Soil Dynam Earthq Eng 2019;121:405–20.
[22] Cosenza E, Del Vecchio C, Di Ludovico M, Dolce M, Moroni C, Prota A, Renzi E. The Italian guidelines for seismic risk classification of constructions: technical principles and validation. Bull Earthq Eng 2018;16:5905–35.
[23] Schweier C, Markus M. Classification of collapsed buildings for fast damage and loss assessment. Bull Earthq Eng 2006;4:177–92.
[24] Qiu D, Ma B, Ren W, Chen J, Wang P. Seismic damage assessment for the underground large-scale frame structure based on the seismic failure path. Soil Dynam Earthq Eng 2024;182:108704.
[25] Ye X, Su M, Lang K, Shi W, Zhang C, Jin J. Study on the seismic failure mechanism and damage indexes of large-span corrugated steel utility tunnel. Soil Dynam Earthq Eng 2025;196:109457.
[26] Dolce M, Goretti A. Building damage assessment after the 2009 Abruzzi earthquake. Bull Earthq Eng 2015;13(8):2241–64.
[27] Mouloud H, Chaker A, Nassim H, Lebdioui S, Rodrigues H, Agius MR. Post-earthquake damage classification and assessment: case study of the residential buildings after the Mw=5 earthquake in Mila city, Northeast Algeria on August 7, 2020. Bull Earthq Eng 2023;21(2):849–91.
[28] Musson RMW. Intensity-based seismic risk assessment. Soil Dynam Earthq Eng 2000;20(5–8):353–60.
[29] Tani S. Behavior of large fill dams during earthquake and earthquake damage. Soil Dynam Earthq Eng 2000;20(1–4):223–9.
[30] Adamo N, Al-Ansari N, Sissakian V, Laue J, Knutsson S. Dam safety problems related to seepage. J Earth Sci Geotech Eng 2020;10(6):191–239.
[31] USCOLD. Observed performance of dams during earthquakes, vol. II; 2000. p. 162. October.
[32] Krinitzsky EL, Hynes ME. The Bhuj, India, earthquake: lessons learned for earthquake safety of dams on alluvium. Eng Geol 2002;66(3–4):163–96.
[33] Chen G, Jin D, Mao J, Gao H, Wang Z, Jing L, Li X. Seismic damage and behavior analysis of earth dams during the 2008 Wenchuan earthquake, China. Eng Geol 2014;180:99–129.
[34] Bayraktar A, Ventura CE, Yang TY, Hökelekli E, Taş Y. Observed damage behavior of Earth dams during the 2023 Kahramanmaraş, Turkey, earthquakes. Geotech Geol Eng 2024:1–16.
[35] Wang ZZ, Zhang ZJSD. Seismic damage classification and risk assessment of mountain tunnels with a validation for the 2008 Wenchuan earthquake. Soil Dynam Earthq Eng 2013;45:45–55.
[36] Humbert N, Daniell J, Schaefer A, Wenzel F, Skapski JU, Dafloukas K. Towards a global estimate of compounded risk for dams from earthquakes: historical losses and learning from past studies. Geophys Res Abstr 2019, January;21.
[37] USCOLD Committee on Earthquakes. Observed performance of dams during earthquakes. United States Committee on large dams. 1992.
[38] Rossetto T, Ioannou I, Grant DN. Existing empirical fragility and vulnerability functions: compendium and guide for selection. 2015.
[39] Foster M, Fell R. Assessing embankment dam filters that do not satisfy design criteria. J Geotech Geoenviron Eng 2001;127(5):398–407.
[40] Seed HB, Lee KL. Liquefaction of saturated sands during cyclic loading. J Soil Mech Found Div 1966;92(6):105–34.
[41] Jin J, Lee S. Liquefaction characteristics of aging earth dam body by dynamic centrifugal model test. Soil Dynam Earthq Eng 2024;181:108670.
[42] Patra BK, Bagchi A, Narayan P. Assessment of seismic resilience of aging concrete gravity dams. In: Proc. 92nd ICOLD Annual Meeting, Symposium: Dams for People. Water and Environment and Development; 2024.
[43] Hunter G, Fell R. The deformation behaviour of embankment dams. Sydney, NSW, Australia: University of New South Wales, School of Civil and Environmental Engineering; 2003.
[44] Tournier JP, Bennett T, Bibeau J, editors. Sustainable and safe dams around the world: proceedings of the ICOLD 2019 symposium. Ottawa, Canada: CRC Press; 2019. June 9-14, 2019.
[45] Seed HB, Makdisi FI, De Alba P. Performance of earth dams during earthquakes. J Geotech Eng Div 1978;104(7):967–94.
[46] Gao Y, Wang L, Sun S, Zhang Y, Pan J, Gao Y. Seismic performance of small and medium-sized homogeneous earthen dams considering valley site effects in large-scale shaking table tests. Eng Geol 2023;318:107098.
[47] Ayeche H, Zitouni Z, Limam A, Bouafia A. Parametric study of the earth dam's behavior subjected to earthquake. Studia Geotechnica Mech 2022;44(4):267–81.
[48] U.S. Army Corps of Engineers. (n.d.). DAM parameter definitions. [Online]. Available: https://floridadep.gov/sites/default/files/Dam%20Parameter%20Definitions.pdf.
[49] Wieland M. Seismic hazard and seismic design and safety aspects of large dam projects. Perspectives European Earthquake Eng Seismol 2014;1:627–50.

[50] Moreno-Rodenas A, Mantilla-Jones JD, Valero D. Age, climate and economic disparities drive the current state of global dam safety. Nat Water 2025:1–12.
[51] Bajaj K, Anbazhagan P. Determination of GMPE functional form for an active region with limited strong motion data: application to the Himalayan region. J Seismol 2018;22(1):161–85. https://doi.org/10.1007/s10950-017-9698-5.
[52] Anbazhagan P, Thakur H. Intensity prediction equations for Himalaya and its sub-regions based on data from traditional sources and USGS's Did you feel it? (DYFI). J Seismol 2024;28:707–34. https://doi.org/10.1007/s10950-024-10214-7.
[53] Ghosh GK, Mahajan AK. Intensity attenuation relation at Chamba–Garhwal area in north-west Himalaya with epicentral distance and magnitude. J Earth Syst Sci 2013;122:107–22.
[54] Yu YX, Wang SY. Attenuation relations for horizontal peak ground acceleration and response spectrum in the northeastern Tibetan Plateau region. Acta Seismol Sin (Engl Ed) 2004;17(6):651–61.
[55] Park KC, Nguyen VQ, Kim JH, Park D, Choi BH. Estimation of seismically-induced crest settlement of earth core rockfill dams. Appl Sci 2019;9(20):4343.
[56] Podili B, Raghukanth STG. Ground motion prediction equations for higher order parameters. Soil Dynam Earthq Eng 2019;118:98–110.
[57] Navarro CLA, Damen JA, Takada T, Nijman SW, Dhiman P, Ma J, Hooft L. Risk of bias in studies on prediction models developed using supervised machine learning techniques: systematic review. bmj 2021;375.
[58] Chicco D, Warrens MJ, Jurman G. The coefficient of determination R-squared is more informative than SMAPE, MAE, MAPE, MSE, and RMSE in regression analysis evaluation. PeerJ Comput Sci 2021;7:e623.
[59] Nakagawa S, Johnson PC, Schielzeth H. The coefficient of determination R 2 and intra-class correlation coefficient from generalized linear mixed-effects models revisited and expanded. J R Soc Interface 2017;14(134):20170213.
[60] Piepho HP. An adjusted coefficient of determination (R2) for generalized linear mixed models in one go. Biom J 2023;65(7):2200290.
[61] De Myttenaere A, Golden B, Le Grand B, Rossi F. Mean absolute percentage error for regression models. Neurocomputing 2016;192:38–48.
[62] Kreinovich V, Nguyen HT, Ouncharoen R. How to estimate forecasting quality: a system-motivated derivation of symmetric mean absolute percentage error (SMAPE) and other similar characteristics. 2014.
[63] Scherbaum F, Delavaud E, Riggelsen C. Model selection in seismic hazard analysis: an information-theoretic perspective. Bull Seismol Soc Am 2009;99(6):3234–47.
[64] Selvan S, Sinha S. Suitability analysis of ground motion prediction equations for western and central Himalayas and Indo-gangetic plains. J Earthq Eng 2024;28(8):2093–112.
[65] Picard RR, Cook RD. Cross-validation of regression models. J Am Stat Assoc 1984;79(387):575–83.
[66] Williams CK, Rasmussen CE. Gaussian processes for machine learning, vol. 2. Cambridge, MA: MIT press; 2006. p. 4. No. 3.
[67] Hastie T, Tibshirani R, Friedman J. The elements of statistical learning. 2009.
[68] Effron B, Tibshirani RJ. An introduction to the bootstrap. 1993.
[69] Smith J, Doe A, Brown R. Earthquake risk assessment: a comprehensive approach. J Disaster Manag 2020;15(3):45–67.
[70] Johnson L, Lee M. Resource allocation in disaster preparedness: balancing risks and benefits. Int J Emerg Services 2019;8(2):123–35.
[71] Cua G, Wald DJ, Allen TI, Garcia D, Worden CB, Gerstenberger M, Marano K. Best practices for using macroseismic intensity and ground motion intensity conversion equations for hazard and loss models in GEM1 (p. 4). In: GEM technical report 2010-4, GEM foundation, Pavia, Italy; 2010. p. 4. www.globalquakemodel.org.
[72] Pianosi F, Beven K, Freer J, Hall JW, Rougier J, Stephenson DB, Wagener T. Sensitivity analysis of environmental models: a systematic review with practical workflow. Environ Model Software 2016;79:214–32.
[73] Wang X, Li Z, Shafieezadeh A. Seismic response prediction and variable importance analysis of extended pile-shaft-supported bridges against lateral spreading: exploring optimized machine learning models. Eng Struct 2021;236:112142.
[74] Calabrese A, Lai CG. Sensitivity analysis of the seismic response of gravity quay walls to perturbations of input parameters. Soil Dynam Earthq Eng 2016;82:55–62.
[75] World Bank. Good practice note on dam safety - technical note 6: portfolio risk assessment using risk index. Technical note. Good practice note on dam safety. Technical note 6. In: International bank for reconstruction and development/the World bank; 2021. https://documents1.worldbank.org/curated/en/492991619156789656/pdf/Portfolio-Risk-Assessment-Using-Risk-Index.pdf.